The syntheses, properties and applications of Si, ZnO, metal, and heterojunction nanowires†

Caofeng Pan and Jing Zhu*

Received 22nd September 2008, Accepted 20th November 2008
First published as an Advance Article on the web 12th January 2009
DOI: 10.1039/b816463k

Great efforts have been made recently to fabricate one-dimensional (1D) nanostructured materials and ordered nanomaterial arrays due to their novel chemical and physical properties for future application in nanodevices. One-dimensional nanostructures, such as nanowires (NWs), nanoribbons and nanotubes, are promising components in a wide range of nanoscale device applications. A large amount of fabrication methods have been developed to synthesize the nanomaterials, such as vapour growth and solution growth processes. In this feature article, we provide a review of some progress in the field of one-dimensional inorganic nanowires, including the syntheses, structures, properties and applications of nanowires and nanowire arrays of Si, ZnO, metals, heterojunctions, etc. materials.

1. Introduction

Since the discovery of carbon nanotubes, there has been great interest in the synthesis, characterization and application of other nanomaterials. Nanomaterials, which are defined with at least one dimension on a scale smaller than 1 micrometer, normally between 1–100 nanometers, have been given a lot of attention due to their special structures, properties and applications superior to those of their bulk materials.

Top-down and bottom-up are two strategies to fabricate nanostructures and devices. The top-down method starts from bulk materials, which are sculpted into nanosized features by carving, milling, etching and patterning. Lithography is one of the most used methods to realize nanostructures in microelectronic engineering for fabricating integrated circuits (ICs). The top-down method can usually achieve good control over the device dimension, location, and organization with high precision. However, high precision induces greater cost when the size of the device is reduced, especially when the size is below 100 nanometers.

In comparison, bottom-up approaches construct structures or devices from basic building blocks, such as atoms, molecules and supermolecular clusters. Bottom-up approaches usually are able to produce devices in parallel and much cheaper than top-down methods. However, it is difficult to obtain large-scale products. A possible solution is to integrate top-down and bottom-up approaches, such as generating large-scale patterns through a lithography technique and controlling the local configuration by a self-assembly process.

Two-dimension materials (films or quantum wells) have been thoroughly investigated for use in fields as diverse as electronic devices and photovoltaic applications in the past two decades

Beijing National Center for Electron Microscopy, The State Key Laboratory of New Ceramics and Fine Processing, Laboratory of Advanced Materials, Department of Materials Science and Engineering, Tsinghua University, Beijing, 100084, China. E-mail: jzhu@mail.tsinghua.edu.cn; Fax: +861062772507; Tel: +861062794026

† This paper is part of a *Journal of Materials Chemistry* theme issue on Nanotubes and Nanowires. Guest editor: Z. L. Wang.

Caofeng Pan

Caofeng Pan holds a BS degree in materials science and engineering and is currently a PhD candidate in the Department of Materials Science and Engineering in Tsinghua University. His PhD thesis has mainly been focused on the synthesis, characterization, properties and novel devices of nanomaterials. He first reported nanowire-based nanofuel cells which can serve as the power supply of nanodevices, and has focused on developing nanopower sources, such as nano-fuel cells and nano-solar cells.

Jing Zhu

Jing Zhu, Professor in Department of Material Science and Engineering, joined Tsinghua University in 1996. She was selected as an academician of the Chinese Academy of Sciences in 1995 and a Fellow of the academy of sciences for the developing world in 2007. Prof. Zhu is one of the pioneers in the analytical electron microscopy field in China. Her research interests include nanomaterials and nanostructures, electron microscopy in materials science, interfaces and surfaces in materials, and research and development of in-situ specimen holders in electron microscopes.

because they can be easily prepared by a lot of commercial techniques such as molecular beam epitaxy (MBE), UHCVD, MOCVD, etc.

Zero-dimensional nanostructures (quantum dots and nanoparticles), which are confined in all three dimensions, have been extensively studied. A large number of chemical and physical methods have been developed to fabricate nanodots or quantum dots with controlled shape and size and from a rich variety of materials.[1] Significant progress has also been made not only in the size dependent physical and chemical properties, but also in fabricating devices using nano (quantum) dots as key components, such as quantum dot lasers, sensors, optical detectors, and single electron transistors, etc.[2]

One-dimensional nanomaterials include nanowires, nanorods, fibers, nanocables, nanotubes, nanobelts and so on. Nanowires, which will be the main focus of this paper, have attracted tremendous interest over the past several years. These nanowire structures provide ideal systems for studying transport processes of one-dimensionally confined objects and related fundamental phenomena, and they are also very important for developing new generation nanodevices with high performance.

Many effective methods have been developed for synthesizing nanowires with well controlled structures, such as arc-discharge,[3] chemical vapour deposition (CVD),[47] laser ablation,[4] electrochemical deposition,[5] sol–gel,[6] template-assisted growth,[7] electrospinning[8] and combinations of the above mentioned methods. In the meantime, a large quantity of 1D nanomaterials with different components and varied structures have been reported, such as carbon nanotubes,[9] elemental materials (Si,[10] Ge,[4,11] B,[12] etc.), binary oxides (SiO_2,[10,13] Ga_2O_3,[14] MgO,[15] TiO_2,[16] tungsten oxide,[17] etc.), nitrides (GaN,[18] AlN,[19] BN[20] and InN[21]), borides (CeB_6[22] and LaB_6[23]), metal carbides (TiC, NbC, Fe_3C, SiC, and BC_x[24]), metal chalcogenides (CdS,[25] CdSe,[26] CdTe,[27] PbS,[28] PbSe,[29] CuS,[30] CuSe,[31] Ag_2Se,[32] NiS[33] and NbS_2,[34] etc.), ternary materials ($BaTiO_3$, $SrTiO_3$,[35] $K_2Ti_6O_{13}$,[36] etc.), metal nanorods (Au,[37] Ag,[38] Pt,[39] Cu,[40] etc.), barcoded metal nanowires,[41] heterojunction nanowires,[74–84] organic nanowires,[42] composite nanostructures[43] and other semiconductor nanowires (GaAs,[44] InP[45] and GaP,[46] etc.) and semiconductor nanobelts.[47] Now an increasing number of nanowires are expected to be produced with the improvement of present synthesis methods and the development of new techniques.

In this feature article, we provide a review of some progress in some 1D inorganic nanowires, such as Si, metal, heterojunctions, ZnO, etc. Firstly, we introduce the synthesis methods developed by us for these inorganic 1D materials, including metal assisted chemical etching, template assisted electrochemical deposition, CVD and so on; secondly, the studies on the special electrical and mechanical properties of the nanowires are discussed in section 3; finally, some applications of our nanowires are demonstrated in section 4.

2. Synthesis and characterization

2.1 Silicon nanowire arrays fabricated by metal-assisted chemical etching method

Similar to carbon nanotubes, another "star material" is silicon nanowires, which have been the focus of a large amount of research in the late 1990s.[48] Silicon nanowires are attracting much attention due to their technical compatibility with existing semiconductor technology. Various morphologies of Si nanostructures have been obtained, such as random orientation nanowires, vertically aligned nanowires,[49] axial and radial heterostructures,[50] nanowires assembled in micro-sized semispheres,[51] etc.

One of the main synthesis techniques for the growth of Si nanowires is physical vapor deposition (PVD). With this method, a source material, usually high purity silicon[10] or silicon dioxide,[52] is sublimed with laser ablation[4] or elevated temperature evaporation.[10] The vapor is then transported to a cool zone where it deposits in the form of silicon nanowires. Chemical vapor deposition (CVD) is another technique for the synthesis of Si nanowires.[53]

Several mechanisms have been proposed for the growth of SiNWs: vapor-liquid-solid (VLS),[54] solid-liquid-solid (SLS),[55] solution-solid-solid,[56] vapor-solid-solid (VSS),[57] and oxide-assisted growth (OAG)[58] mechanisms. In most cases the growth of silicon nanowires is facilitated by a metal catalyst and follows a VLS process, this catalyst confined nanostructure growth has been proven to be an effective method for precise size control.[53] However, these growth mechanisms show some limitations in practice, for example, they generally need high temperatures (900–1100 °C) or a high vacuum, templates and complex equipment, and sometimes they employ hazardous silicon precursors (such as SiH_4 or $SiCl_4$).

We have developed a novel, metal-assisted chemical etching method to fabricate ordered large-area SiNW arrays.[59] Combining electroless metal deposition (EMD) with the chemical etching mechanism, the large-area SiNWs were prepared successfully on silicon substrates in aqueous HF solution containing appropriate amounts of $AgNO_3$. The etching depth (length of SiNWs) could be tuned by adjusting the etching time. This new technique has the advantages of mild preparation conditions, low synthetic temperature, simple equipment and time-saving over other techniques such as CVD and laser ablation. Large-area SiNW arrays are firstly obtained near room temperature using this method.

In particular, the metal-assisted chemical etching method has been used to fabricate SiNW arrays of pre-determined properties from parent silicon wafers. Nanowires synthesized by this approach are vertically aligned (Fig. 1a) with controlled n- or p-type doping, controlled crystallographic orientation (including [111] (Fig. 1b), [100] (Fig. 1c) *etc.*) and consistent throughout batches, and across large areas up to wafer-scale.

It is very important to clarify the growth mechanics of the metal-assisted etching. To date, there still are some different opinions, some people believe that the catalyst (Ag or Au, etc.) protects the silicon underneath from being etched,[60] while others insist that catalyst particles only catalyze etching of the Si substrate in contact with them.[61] Thus, it is necessary to carry out some investigations of the detailed mechanism of metal assisted etching on Si.

A method involving dry deposition plus wet chemical etching was also devised to fabricate SiNW arrays and to study silver catalysis during fabrication.[62] The investigation of the track of catalyst particles showed that Ag really catalyses the etching of the silicon underneath it, which clarifies the doubts about the

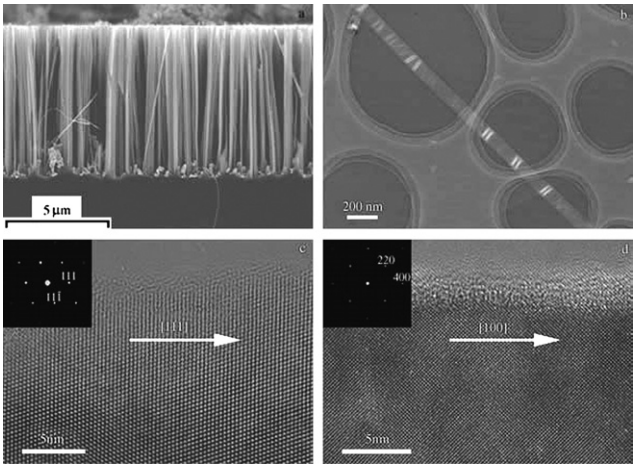

Fig. 1 a) SEM cross-section image of silicon nanowire arrays. b) TEM image of an individual SiNW prepared from a p-type (111)-oriented silicon substrate. c) High-resolution transmission electron microscopy (HRTEM) image of the nanowire in b) (the inset is the ED pattern recorded along the [−1−10] axis). d) HRTEM image of a nanowire synthesized from a p-type (100)-oriented silicon substrate (the inset is its ED pattern recorded along the [001] axis) (ref. 59).

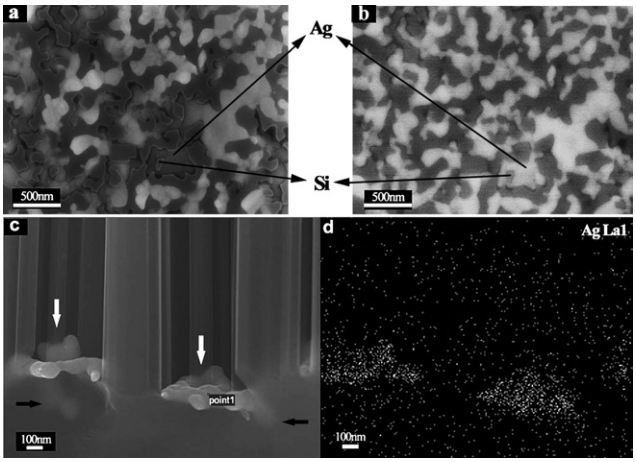

Fig. 2 (a) Secondary electron image and (b) back-scattering electron image of the same planar area. (c,d) Cross-sectional view of the bottom of SiNWs for a longer etching time. (c) SE image (SEM accelerating voltage = 15 kV); (d) EDS mapping result of Ag corresponding to (c) (ref. 62).

formation of SiNW arrays during wet chemical etching. Secondary electron (SE) images, back-scattering electron (BSE) images and the EDS mapping image of the same area of the sample are shown in Fig. 2. By comparison of Fig. 2(a,b), it can be concluded that the silicon under the Ag nanoclusters is first etched off to form shallow pits, so that the Ag clusters sink into the pits. The silicon which was not covered with Ag remains unchanged, and with the sinking of the surrounding network composed of Ag clusters these silicon areas protrude to be nanowires after etching for a longer time (generally about 10 min). The cross-sectional view of the bottom of SiNWs and the EDS mapping of Ag are shown in Fig. 2(c) and (d), which strongly support the conclusion that in our system Ag really catalyses the etching of silicon underneath it, finally to form SiNW arrays.

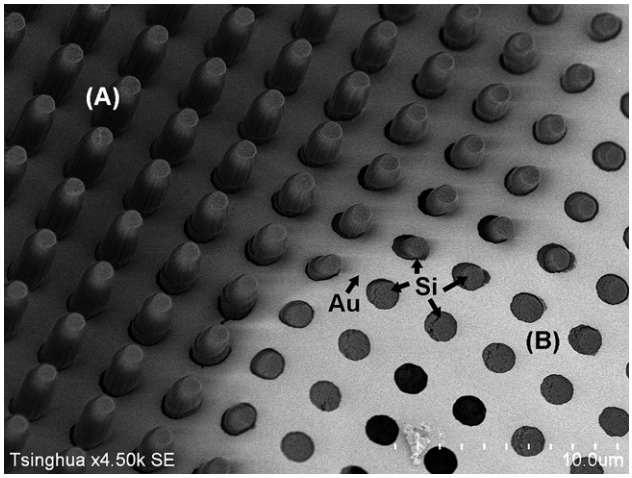

Fig. 3 A SEM image show the mechanism of metal assisted etching.

The latter mechanism that the catalyst particles only catalyze etching of the Si substrate in contact with them is further proved by the latest investigations in our lab, shown in Fig. 3. A gold film with a hexagonal array of holes as a catalyst can be obtained by thermal evaporation onto the silicon substrate and can then work as a catalyst. Afterwards the sample was immersed into an etching solution—a mixture of deionized water, HF, and H_2O_2. Fig. 3 shows a specific area which contains different areas with different etching speeds. The upper-left part (labeled with (A)) has a faster etching speed while the lower right corner (labeled with (B)) has a slower etching speed. It is obviously that the Au film catalyzes etching of silicon beneath it. During the etching process, the "walls" of the honeycomb are gradually etched away and the remnant silicon forms a nanowire array. This result is very strong proof to support the mechanism that the catalyst particles only catalyze etching of the Si substrate in contact with them.

By understanding the metal-catalytic etching mechanism, we have developed this method in order to fabricate controlled large-scale ordered silicon nanowire arrays, by which the diameter, the height of individual nanowires, and the center-to-center distance between nanowires can be controlled accurately.[63] The overall fabrication process is schematically depicted in Fig. 4.

Fig. 5 (a) and (b) show plane-view and tilted-view (*ca.* 15°) SEM images of silicon nanowire arrays fabricated using PS

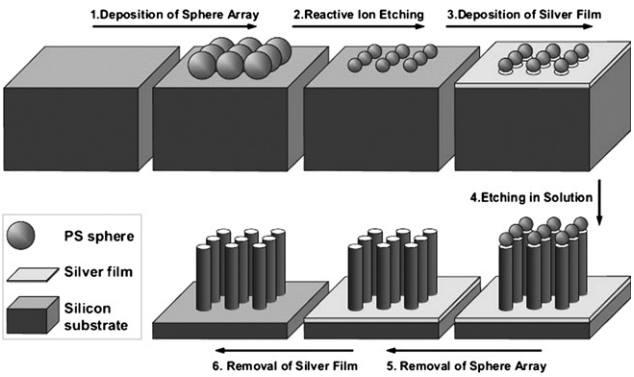

Fig. 4 Schematic depiction of the fabrication process.

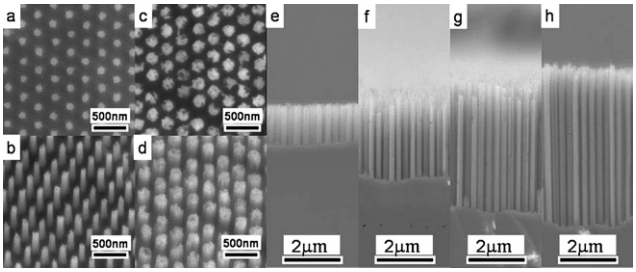

Fig. 5 SEM images of samples where PS spheres with a nominal diameter of 260 nm have been used. Plane-view and tilted-view (*ca.* 15°) images of samples fabricated using PS spheres with a reduced diameter of a,b) 100 nm and c,d) 180 nm. Cross-sectional SEM images of samples after etching for e) 4 min, f) 8 min, g) 12 min, and h) 16 min (ref. 63).

spheres with a reduced diameter of 100 nm as the template; Fig. 5 (c) and (d) show nanowires fabricated using PS spheres with a reduced diameter of 180 nm. These results show that the diameter of the silicon nanowires can be controlled by selecting PS spheres with the desired reduced diameter. Another parameter of the silicon nanowire arrays, the length, is related to the duration of the etching process. Fig. 5 (e–h) show cross-sectional SEM images of silicon nanowires fabricated with etching times of 4, 8, 12, and 16 min, yielding nanowires with lengths of *ca.* 1.3, 2.7, 4.5, and 5.3 μm, respectively. The length of the nanowires varies linearly with the duration of the etching process, which provides relatively precise control over the length of the nanowire arrays.

Note that the most important difference between those Si NWs prepared using the VLS method and the metal-assisted chemical etching method is the roughness of the surface. The mean roughness height of metal-assisted chemical etched nanowires varied from wire to wire, but was typically 1–5 nm with a roughness period of the order of several nanometres, while the VLS prepared nanowires have a relatively smooth surface, which can be seen in Fig. 6. This roughness may be attributed to randomness of the lateral oxidation and etching in the corrosive aqueous solution or slow HF etching and faceting of the lattice during synthesis.

It was found that for the chemical etched nanowires, the roughness at the nanowire surface behaves like secondary scattering phases. The roughness may contribute to higher rates of diffuse reflection or back scattering of phonons at the interfaces. Because this scattering of phonons will greatly reduce thermal conductivity without much affecting the Seebeck coefficient and electrical resistivity, it makes Si nanowire arrays show promise as high-performance, scalable thermoelectric materials.[64]

2.2 Template-assisted synthesis

Template-assisted synthesis represents a convenient and versatile method for generating 1D nanostructures. In this technique, the *in situ* fabricated material is shaped into a nanostructure with morphology complementary to that of the template. The templates could be nanoscale channels within mesoporous materials, anodic alumina oxide membranes (AAO) and polycarbonate membranes. The nanoscale channels are filled using the CVD method, the solution, the sol-gel or the electrochemical

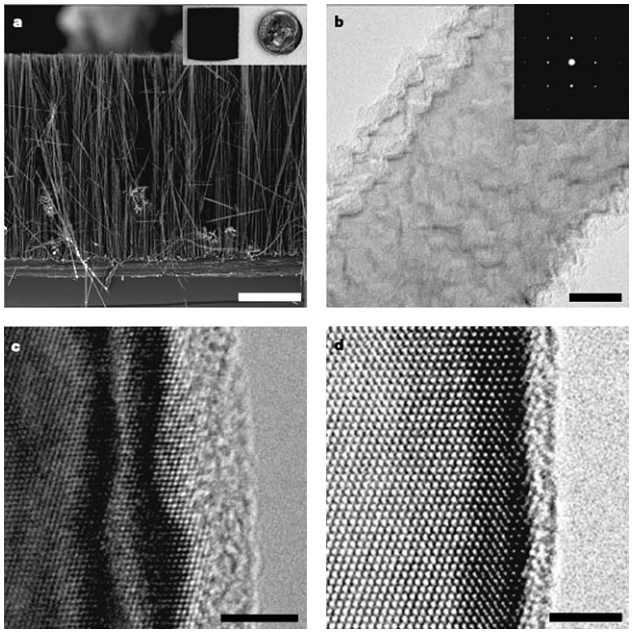

Fig. 6 Structural characterization of the rough silicon nanowires. a, Cross-sectional SEM of an electroless etching Si nanowire array. b, Bright-field TEM image of a segment of a metal-assisted chemical etched Si nanowire. c, High resolution TEM image of a metal-assisted chemical etched Si nanowire. The roughness is evident at the interface between the crystalline Si core and the amorphous native oxide at the surface, and by undulations of the alternating light/dark thickness fringes near the edge. d, High-resolution TEM of a VLS-grown Si nanowire. Scale bars for a–d are 10 mm, 20 nm, 4nm and 3 nm, respectively (ref. 64).

method. The nanowires can be released from the templates by removal of the host matrix.[65]

Although a lot of templates, such as polymer membranes, mesoporous silica, nanowires or nanotubes, have been demonstrated by different groups, the most commonly used one is AAO. Unlike the polymer membranes fabricated by track etching, AAO contains a hexagonally packed 2D array of cylindrical pores with a uniform size (Fig. 7). The AAO templates can be fabricated by a two-step anodization process. It is proved that 4% oxalic acid solution is suitable for preparing templates with pore diameter from 70nm to 110nm, while 10% H_2SO_4 is for those of smaller pores. In most cases, the pore size of AAO is about 30 to 110 nm, but by applying comparatively lower anodizing potentials of 6–18 V, AAO membranes with pore diameters varying from 6 to 19 nm can be obtained.[66] In this case, the interpore distance is proportional to the applied anodizing potential and varies in the range of 20–58 nm, which can be used to fabricate 1D nanomaterial arrays of high density. A linear relationship between the anodizing potential (U_a) and the interpore distance (D_{int}) was also revealed: $D_{int} = 2.97U_a + 2.49$, shown in Fig. 7(c). Further studies show that AAO membranes with large ordered pore domains can be successfully prepared by the annealling pre-treatment of polycrystalline aluminium sheets.[67]

Using AAO as a template, a large number of materials have been fabricated to form nanowires, including Au, Ag, Pt, Ni, Fe, Cu, Co, Si, TiO_2, MnO_2, ZnO, SnO_2, In_2O_3, CdS, CdSe, CdTe and conducting polymers (polypyrole, polyaniline, etc.), as well as carbon nanotubules.

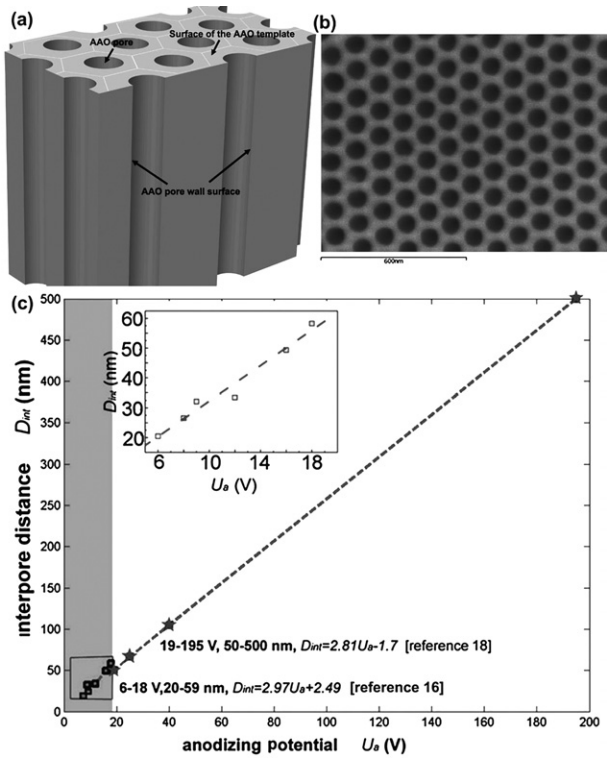

Fig. 7 (a) A scheme of AAO templates. (b) A SEM image of as prepared AAO (top view). (c) Relationship of the interpore distance (D_{int}) and the anodizing potential (U_a). Data from the present work are plotted in the shaded zone, fitting to a formula of $D_{int} = 2.97U_a + 2.49$, while data from ref. 68 are plotted in the white zone with another fitting formula of $D_{int} = 2.81U_a - 1.7$ for comparison. The inset shows a magnified view of the rectangle-enclosed part. The interpore diameters are 20.47, 25.89, 32.13, 33.49, 49.33, and 58.25 nm under lower anodizing voltages of 6, 8, 9, 12, 16 and 18 V, respectively (ref. 66).

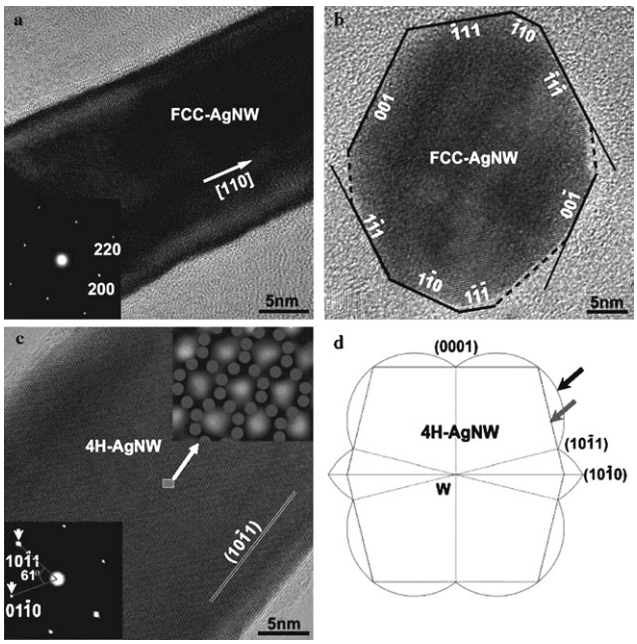

Fig. 8 (a) HRTEM image of a FCC-AgNW, with a longitudinal axis [110]. The inset is an electron diffraction pattern from this nanowire indexed as FCC-Ag. (b) An image of the cross section of a FCC-AgNW. The cross section is perpendicular to the longitudinal axis [110] of the nanowire and shows that the surfaces of the nanowire are base, {001}, and {110} planes. Dashed lines represent some other facets consisting of planes with orientations close to the low-index planes (about 20° angles, indicated by elongate solid lines). (c) High-resolution TEM image of a single crystalline 4H-AgNW. The lower left inset is an electron diffraction pattern from the 4H-AgNW. The zone axis of this electron diffraction pattern is [−2113]. Besides, the electron diffraction pattern shows that the (10−11) plane is parallel to the axis of the nanowire. The upper right inset is a magnification of the area marked by a white rectangle in c, where some dots are added to show the atomic projection of 4H-Ag along [−2113]. (d) The calculated cross section of a 4H-AgNW by the broken-bond rule and Wulff's construction, where the surface energy curve is marked with a black arrow and the surfaces of the nanowire are marked with a grey arrow and terminated by {0001} and {10−11} planes (ref. 71).

Since various nanowires fabricated *via* template-assisted methods have been reported in so many papers and reviews, herein we will mainly focus on some unique work developed in our group, such as polytypic Ag and Ni nanowires.

2.2.1 4H and FCC polytypic Ag nanowires. Silver has attracted a lot of attention because it has the highest electrical conductivity among all metals at room temperature. Highly ordered AgNW arrays have been obtained by various methods, such as solution based growth[69] and electro-chemical deposition into AAO templates.[70]

However, it is the first time that we discovered 4H-AgNWs (Fig. 8c) coexist with FCC-AgNWs (Fig. 8a) with diameters ranging between 8–100 nm.[71] Based on the thorough investigation into the crystal structures of 4H- and FCC-AgNWs, a size dependence of the crystal structure in AgNWs was discovered. The 4H-AgNW concentration reaches the highest value (52%) in the AgNWs with diameters around 30 nm, decreases from 52% to 17% in the 50 nm AgNWs and 14% in the 75 nm ones, and is expected to approach zero when the nanowire diameters go even larger than 75 nm.

Based on the crystallographic characteristics of both 4H- and FCC-AgNWs, the systemic energy of an individual AgNW, that is, the sum of internal energy and surface energy, is analyzed. It was revealed that 4H-AgNW had a favorable surface configuration but unfavorable internal energy compared to FCC-AgNW, leading to a lower systemic energy of 4H-AgNW in the proper diameter range around 30 nm. This also accounts for the absence of 4H-Ag in the bulk where the specific surface area is very low. Similar phenomena may exist in some other systems, and the dynamical process needs further studies.

2.2.2 FCC and HCP Ni nanowires. Nickel nanowire arrays have potential applications in perpendicular magnetic recording, microwave absorption and magnetic nanodevices. In these applications, high coercivity (Hc//) and squareness (S//) parallel to the nanowire direction are much concerned. Direct current (DC) electrodeposition in AAO templates is an important method to fabricate Ni nanowire arrays.[72] However, the Ni nanowire arrays made in this way always show low S//. Some new methods have been developed to solve the problem.[73]

During the electrodeposition process, magnetic stirring and an external magnetic field were applied, as shown in Fig. 9a. It has

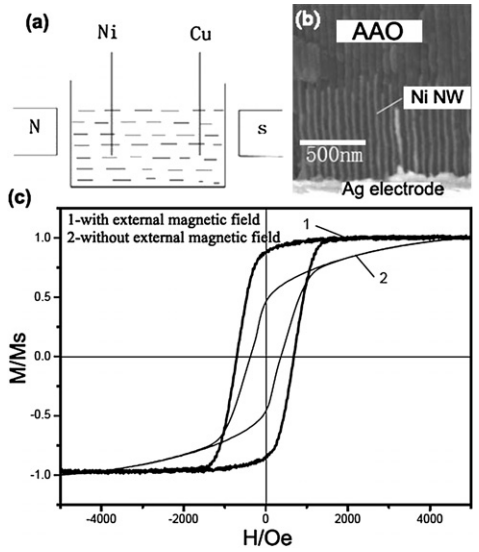

Fig. 9 (a) A demonstration of the magnetic field assisted Ni NW synthesis process, (b) a SEM cross section view of a Ni NW filled AAO template, (c) the M-H loops of the Ni nanowire array: 1 with and 2 without an external magnetic field applied in deposition (ref. 73).

been proved that this method can improve the S// markedly. By far, the S// of the nanowire arrays made in this method can reach as high as 0.93.

Another approach in improving the S// is making single crystal Ni nanowires. As is well known, one of the drawbacks of template-assisted synthesis is that it is difficult to obtain materials in single crystal form. Under a high-current deposition, single crystalline Ni nanowire arrays have been successfully fabricated, and the S// of nanowires made in this method approaches 1. Further studies show that a preferred orientation of (220) will occur if the deposition voltage is higher than 3V. In addition, some HCP Ni nanowires are reported for the first time with a preferred orientation of (220). With heat treatment, the phase transition from HCP Ni NWs to FCC Ni NWs is observed for the first time in Ni nanowires (Fig. 10).

2.3 1D heterostructured nanomaterials

In modern microelectronics, heterostructures are significant for all kinds of devices and integrated systems due to their roles as either functional or interconnecting elements. Therefore, research on 1D heterojunctions is necessary for nanoelectronics. At present, many kinds of 1D heterojunctions have been reported, such as Si/CNT (carbon nanotube),[74] CNT/SiC,[75] CNT/TiC,[75] Si/SiGe,[76] InAs/InP,[77] GaAs/GaP,[78] rectifying junctions in metal nanowires,[79] Au/ZnO,[80] metal/CdSe/metal,[81] NiSi/Si,[82] In/Si[83] and so on.

In our group, ordered arrays of four kinds of 1D heterojunctions, including Ni/MWCNT (multi-walled CNT)/a-CNT (amorphous CNT), Ag/a-CNT, Ag/Si and Pt_6Si_5/Si, have been synthesized by a combination of electrochemical deposition and CVD with AAO membranes as templates.[84] Of these 1D heterojunctions, each consists of two or three different nanowires/tubes connected end to end. Their structures have been characterized clearly.

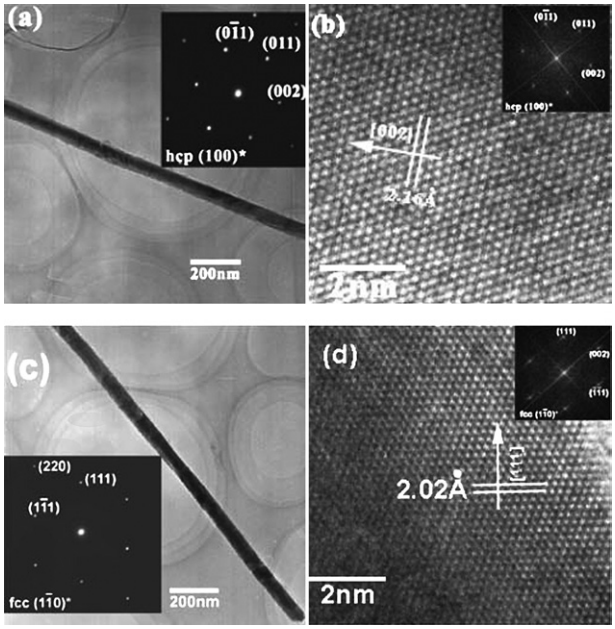

Fig. 10 (a, b) TEM images of HCP Ni found in the sample without heat treatment. (a) A segment of HCP Ni. The inset is the selected area electron diffraction pattern (SAED). (b) HRTEM image and its fast Fourier transition (FFT, inset). TEM observations show that HCP Ni nanowires or segments have no preferred orientation. (c, d) TEM micrographs of FCC Ni nanowire after heat treatment. (c) A FCC nanowire and the SAED (inset). (d) HRTEM image and FFT (inset). The FCC Ni nanowires show (220) preferred orientation (ref. 73).

Particularly, the Ni/MWCNT/a-CNT structure is found to be extraordinary. In each Ni/MWCNT/a-CNT 1D heterojunction (Fig. 11), each wall of the MWCNT is in direct contact with the tip of the Ni nanowire at the Ni/MWCNT interface, and multiple outer walls of the MWCNT are contacted by the a-CNT at

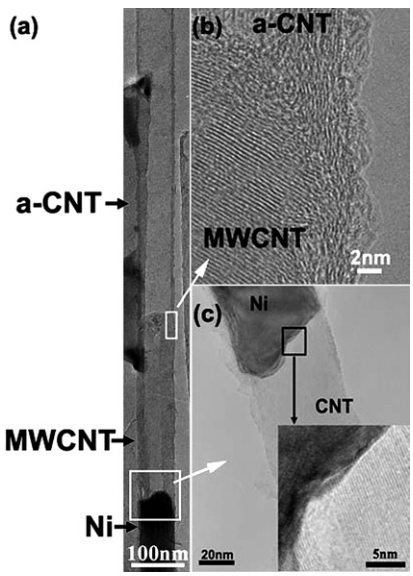

Fig. 11 (a) TEM image of a typical Ni/MWCNT/a-CNT 1D heterojunction. (b,c) High-resolution TEM image of the interfacial structure of the Ni/MWCNT and MWCNT/a-CNT contact (ref. 84).

the MWCNT/a-CNT interface. This control of interfacial structures enables multiple outer walls of a MWCNT to participate in electrical transport simultaneously, which is unique.

Furthermore, in the study on characterization of the chirality of MWCNTs, HRTEM images of the sidewall and the core regions of MWCNTs, where confusions easily occur, have been analyzed. It is demonstrated that the sidewall images are not structural ones and obtained by the interference of the {0002} and the {10−10} diffraction waves. The core images are more favorable for the analysis of the MWCNT chirality.[85]

A Ag–Si nanowire heterojunction is shown in Fig. 12 (a,b), the diameter is predominant around 90nm, which corresponds to the size of the AAO template pores. The HRTEM image shown in Fig. 12b is from the interface area of the individual nanowire junction shown in Fig. 12a. From the HRTEM image we can see that there are three parts: the Ag part, the interface Si–Ag solid solution, and the Si part. There is no amorphous layer in the interface.

AgNW/a-CNT heterojunction arrays were also obtained in our group, which are shown in Fig. 12 (c–e). A SEM image of the cross section view of a AgNW/a-CNT heterojunction array is shown in Fig. 12d. Fig. 12c shows a TEM image of a heterojunction node, and its corresponding HRTEM image is shown in Fig. 12e. It is obvious that each heterojunction is composed of a single-crystal AgNW and an a-CNT that consists of many tiny carbon clusters. The amorphous nature of the latter is due to its growth mechanism, which is based on self-catalytic functions of the AAO channels. The contacts between the a-CNTs and the Ag nanowires in the Ag/a-CNT 1D heterojunctions are shown to be ohmic, which derive from general characteristics of the energy band structure of amorphous semiconductors. It will be further discussed in section 3.1.2.

A TEM image of a Pt_6Si_5/Si 1D heterojunction is illustrated in Fig. 12f. According to our electron diffraction analysis, the dark part of the heterojunction is identified as Pt_6Si_5 and the light end is identified as Si. In every Pt_6Si_5/Si 1D heterojunction, the single-crystal Pt_6Si_5 nanowire is synthesized by using a polycrystalline Pt nanowire, which offers a new method to synthesize metal silicide nanowires.

The electronic properties of these 1D heterojunctions will be discussed in the following section.

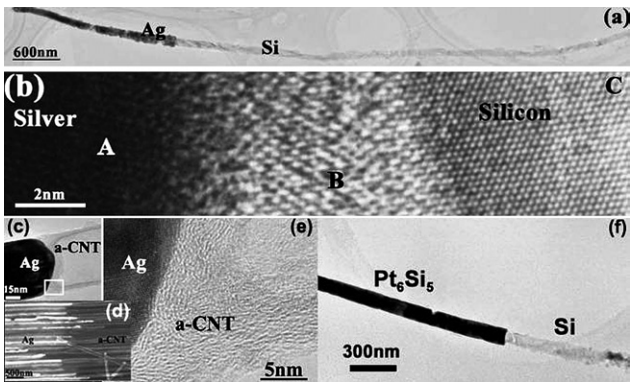

Fig. 12 (a) TEM image of an Ag/Si 1D heterojunction; (b) HRTEM image from the interface area of the heterojunction in (a); (c) transmission electron microscope (TEM) image of an Ag/a-CNT 1D heterojunction; (d) SEM image of the cross section view of the AgNW/a-CNT heterojunction array; (e) HRTEM image of the area marked with the white box in (c). In addition, twins and stacking faults exist in the Ag nanowire in (c), which are reflected in (d); (f) a TEM image of a Pt_6Si_5/Si 1D heterojunction (ref. 84).

2.4 Vapor phase growth of nanowires

Vapor phase growth is extensively used for producing nanowires. Both elemental and compound nanowires can be obtained *via* this method by choosing appropriate starting materials and suitable reaction conditions. In most of these cases, the mechanisms can be attribute to VLS, VS, VSS, OAG, etc.

A simple method to synthesize nanowires was developed by our group. By heating raw materials directly at suitable temperatures and ambient pressure in certain flow rates of gases and without catalyst, nanowires with diameters less than 100 nm are fabricated, including Si_3N_4, SiC, Ga_2O_3, GaN, ZnO, AlN nanowires and amorphous SiO_2 nanowires.[86] The growth mechanism of these nanowires were investigated and attributed to the VS growth process.

Herein we mainly focus on the fabrication of nano/microsized ZnO rods and arrays. As is well known, since the new century, the study of 1D nanostructured ZnO has been increasing dramatically owing to its unique properties, and many potential applications in devices. A large number of methods have been reported for fabricating ZnO nanostructures.[87] Some potential applications based on various ZnO nanostructures, *e.g.* nanowire nanogenerators, have recently been developed.[107]

But it is still a great challenge to overcome difficulties in fabricating a low dimensional material with wider scale from nanometer to micrometer in a one-step process. It has been reported that nano and micro ZnO rods and arrays have been synthesized through a simple thermal evaporation approach on a cylinder-shaped substrate by heating Zn powders directly.[88] Fig. 13 shows the SEM images of ZnO rods and arrays synthesized on a iron wire substrate. Fig. 13a shows a large area of individual protrusive ZnO rods with varied diameters and lengths. The upper left and right insets of Fig. 13a are images with large magnification at some places of the substrate, showing areas of several individual ZnO nanorods with different lengths and one uniform rod of 400 nm in diameter and 11μm in length, respectively. Fig. 13b is a top view of a large area of well-aligned ZnO nanorod arrays. Such arrays can extend about 3 to 5 mm along the substrate. The upper left and right insets of Fig. 13b show the areas of microsized and nanosized rod arrays, respectively. Well-aligned ZnO rods can be acquired at the place about 6cm downstream or 7cm upstream of the source while the Ar flow is 180 sccm and the heating temperature is 675 °C. In the well-aligned arrays, the diameters and the lengths of the ZnO rods range from 17 nm to 1.2 μm and from 4 μm to 10 μm, respectively. In particular, a special area is shown in Fig. 13c where the diameters of ZnO rod arrays decrease from micrometer to nanometer. The sharp boundary has been seen often in our products. Further work has also been done on how to exactly control the diameters of ZnO rods and how to fabricate varied morphologies made up of ZnO rods. It can be seen from the inset picture of Fig. 13c that ZnO structures have hexagonal cross sections, which is typical of the [0001] direction of a ZnO rod. The perfect crystalline ZnO rods with different scales from

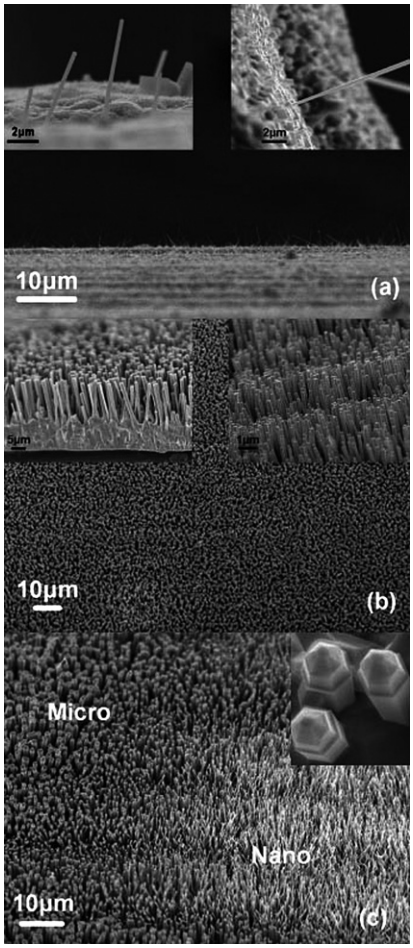

Fig. 13 SEM images of the as-synthesized individual ZnO rods and arrays obtained from Zn powder thermal evaporation deposition on iron wire substrate: (a) individual protrusive ZnO nanorods, the upper left and right insets are images with large magnification at some places of the iron wire, showing areas of several individual ZnO nanorods with different lengths and one uniform rod of 400 nm in diameter with 11 μm in length, respectively; (b) large area of well-aligned ZnO rod arrays, the upper left and right insets show areas of microsized and nanosized rod arrays, respectively; (c) a mixture area of nano/micro ZnO rod arrays (ref. 88).

nanometer to micrometer are good models for the investigation of fundamental concepts about the effects of dimensionality and size on, for example, mechanical, optical, and electrical properties. The size dependence of Young's modulus in ZnO nanowires will be discussed in the following section.

3. Properties of inorganic nanowires

3.1 Electrical properties of 1D inorganic nanowires (arrays)

Electrical/transport properties of nanowires always come with a unique one-dimensional carrier transport mechanism, and its understanding is important in the electronic applications. Important parameters such as wire diameter, wire surface condition, crystal structure and its quality, chemical composition, and crystallographic orientation along the wire axis etc. have been noticed that influence the electron transport mechanism of nanowires.

It has been reported that both ballistic and diffusive type electron transport mechanisms exist in nanowires, and depend upon the wire length and diameter. The ballistic type transport phenomenon is associated with predominant carrier flow without scattering, wherein the carrier mean free path is longer than the wire length.[89] In the diffusive type conduction mechanism, the carrier mean free path is smaller than the wire length.

At the nanoscale level those surface-related properties are more significant, and can even be dominant, for the simple fact that with decreasing the characteristic material size a greater percentage of the atoms/molecules in a given sample/structure are located on the surface region. Therefore, the large surface-to-volume ratio is expected to play a major role in determining the properties and characteristics of nanostructures. It is already recognized that the properties of nanostructures depend sensitively on surface composition and surface states/defects. For example, Lu *et al.* reported that thin ZnO nanowires have significantly higher conductivity due to enrichment of surface states.[90] Lieber *et al.* reported that surface modification of silicon nanowires (SiNWs) could lead to remarkable enhancement of mobility.[91] Lewis *et al.* showed the fabrication of high-performance air-stable SiNW FETs by modifying the surfaces of SiNWs with Si–CH_3 functionality.[92] It has been also pointed out that surface scattering plays a dominant role in the transport properties of small-diameter NWs (<100 nm), whereas transport in intermediate diameter (120–180 nm) NWs is dominated by grain boundary scattering.[93]

Furthermore, it is found that the conductance of nanowires strongly depends on their crystalline structure. For example, in the case of perfect crystalline Si nanowires having four atoms per unit cell, generally three conductance channels are found. In the following part, we will introduce another example of the electrical measurement of polytypic AgNWs and some heterojunctions.

3.1.1 *In situ* electrical study of polytypic silver nanowires. The size-dependent crystallographic structure of Ag nanowires was revealed and novel 4H structure silver nanowires (4H-AgNWs) have been reported to coexist with the usual face-centered cubic (FCC) ones.

Here we discuss the electrical properties of these polytypic AgNWs.[94] *In situ* electrical measurement of the polytypic AgNWs was carried out in a structure-resolved way using a STM inside a TEM. In the diameter range of 20–80 nm, both the 4H- and the FCC-AgNWs are metallic conductors, with comparable average resistivity of 19.9 μΩ cm and 11.9 μΩ cm, respectively; both are one magnitude higher than the 1.6 μΩ cm of bulk FCC-Ag.

The failure of the AgNW under large current stress was accompanied by intense atomic diffusion on the surfaces at a critical current density up to 10^8A/cm^2. Saturation in current, as usually seen in bulk metals due to the positive temperature coefficient of the resistance, was never observed for all AgNWs. This is consistent with the resistance mechanism dominated by surface scatterings. We proposed a parameter, the maximum stable current density (MSCD), to estimate the current-carrying ability of the AgNWs.

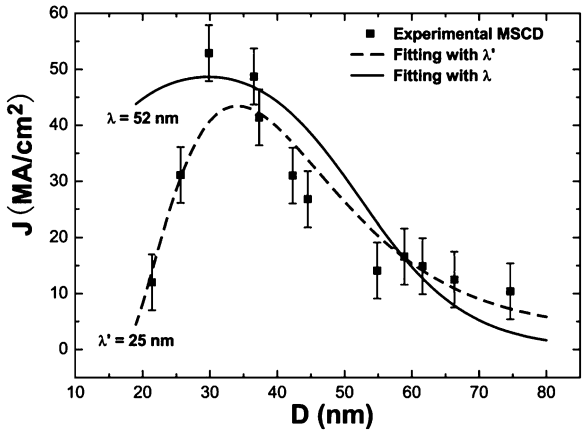

Fig. 14 Diameter dependence of the maximum stable current density (MSCD, J). The fitting curve in a solid line is based on the assumption that the bulk mean free path (MFP) holds in the thin AgNWs, $\lambda = 52$ nm, while the fitting curve in a dashed line corresponds to a reduced MFP, $\lambda' = 25$nm. They both predict a peak of MSCD with similar positions close to the experimental one. The transverse magnetic field deflects the conducting electrons in the straight thin AgNWs and enhances surface scattering (ref. 94).

With a sweeping method used in our experiments, we discovered that MSCD of the AgNWs is diameter-dependent, reaching its maximum around 34 nm in diameter and dropping rapidly with smaller diameters. It generally has a magnitude of 10^7A/cm^2 for AgNWs in the diameter range of 20–80 nm, much larger than the 10^3–10^4A/cm^2 for house wiring.

A phenomenological model is proposed to explain this size dependence of the MSCD. Surface effects due to fast annihilation of current-induced vacancies at the surface of NWs as well as enhanced surface scattering were suggested (see Fig. 14).

3.1.2 The electrical properties of some 1D heterojunctions. The electrical properties of individuals of the Ni/MWCNT/a-CNT and the Ag/a-CNT 1D heterojunctions have been measured.[95]

(I) Metal/a-CNT 1D heterojunctions: ohmic contact with a resistant about 10MΩ. The formation of ordered arrays of Ag/a-CNT 1D heterojunctions with filling ratios close to 100% offers a firm base for further studies of these 1D heterojunctions. Thus, we used conductive AFM to measure the electrical properties of the Ag/a-CNT 1D heterojunctions in their arrays, as shown in Fig. 15a. When a voltage of 3V was applied between the AFM tip and the array in a contact mode, a topographic image and a current-sensing image of the array were simultaneously obtained, shown in Fig. 15(b,c), respectively. In Fig. 15(c), most of the heterojunctions were circuited electrically and some were not so, probably because some disconnections existed in their circuits caused by treating the array for the AFM experiments. When the tip was located at a bright point in Fig. 15(c) and so contacted the corresponding heterojunction, current–voltage (I-V) curves of the heterojunction were acquired. Most of these I-V curves are linear. These linear I-V curves indicate that, in the corresponding heterojunctions, the contacts between the Ag nanowires and the a-CNTs are ohmic. This finding has universal

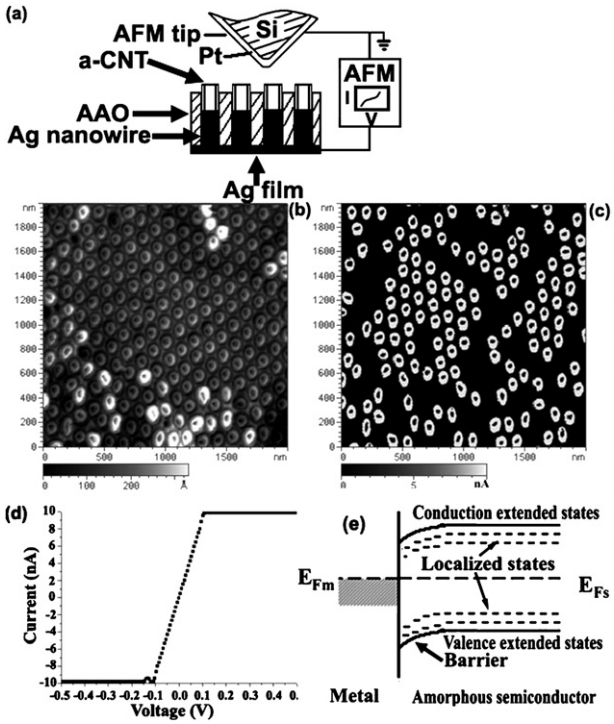

Fig. 15 Schematic for measuring the electrical properties of Ag/a-CNT 1D heterojunctions in an array, which is the same as that in Fig. 12. (b) Topographic AFM image of the array. (c) Current-sensing image corresponding to (b). (d) A typical I-V curve from a heterojunction by the AFM measurement. (e) The schematic of the energy band structure between metal and a-CNT (ref. 95).

significance and offers a wide opportunity for designing large-scale interconnections among nanowires and nanotubes.

(II) Ni/MWCNT/a-CNT 1D heterojunctions. As shown in Fig. 11, multiple outmost walls in the MWCNT of a heterojunction can simultaneously participate in the electrical transport through the Ni/MWCNT and the MWCNT/a-CNT contacts, which is unique. Experimentally, a device configuration as shown in Fig. 16(a) has been prepared. Twelve samples in total were measured by the same method as that in Fig. 16(a). It is found that all of them exhibit reproducible asymmetric and rectifying I-V behaviours, of which one is shown in Fig. 16(b). These I-V characteristics show that the MWCNTs in the measured 1D heterojunctions are all semiconducting and Schottky contacts exist at the two ends as shown in Fig. 16(c). It has been revealed that these Schottky contacts are in accord with the thermionic emission theory in mesoscopic scale and are affected only by the image force. This work is a significant exploration and an effective illustration for the application of the thermionic emission theory in Schottky contacts formed in 1D heterostructured materials.

In addition, the finding that most of the contacts to the MWCNTs in the heterojunctions are the most nearly ideal Schottky diodes is exciting, because it is rather difficult to get nearly ideal diodes, for which many efforts have been made. It should be attributed to the special structures of the heterojunctions, which cause the multiple outmost walls of the

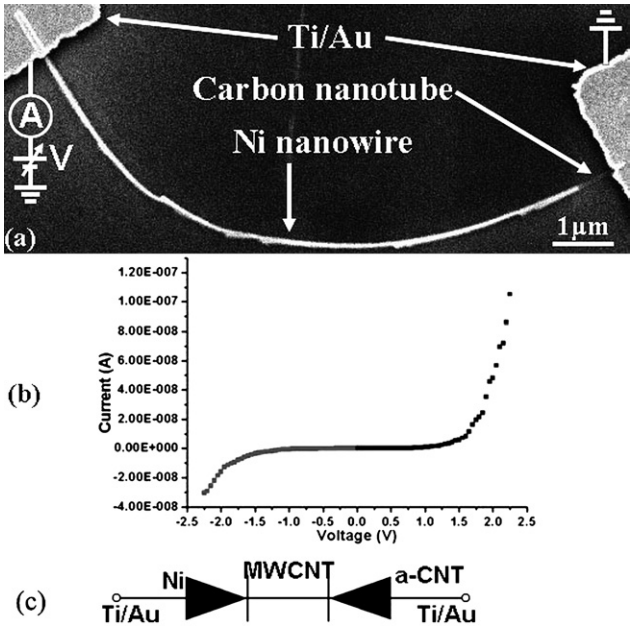

Fig. 16 (a) SEM image of a Ni/MWCNT/a-CNT 1D heterojunction, whose ends are contacted by two Ti/Au electrodes, on the oxide layer of a silicon wafer. Some schematic symbols are added in (a) to show that the left Ti/Au electrode is connected to a pA meter and a DC (direct current) voltage source, and that the right one is to ground. (b) I-V curve obtained by the same configuration as that in (a), where the part with V<0 is in grey and the other is in black. (c) A models for the samples in (a), in which two diodes are connected face to face. According to quantitative theoretical analyses on the I-V data, this model accords with the facts (ref. 95).

MWCNTs to be simultaneously contacted well by the other components of the heterojunctions.

3.2 Mechanical properties of 1D inorganic nanowires

Compared with the extensive study on the electrical properties, mechanical behavior has received much less attention. However, the mechanical properties of nanowires are very important for applying nanowires in NEMS, *etc*.,which has attracted much attention.

Because of the high ratio of surface to bulk atoms and the reduced number of defects, one dimensional systems are expected to have interesting mechanical properties.

The Young's modulus, which is one of the key parameters to evaluate the mechanical properties, is defined as the ratio of stress over strain. Conventional elastic theory indicates that the Young's modulus reflects the average binding forces between the atoms for homogeneous materials. Therefore, at low dimensions, the modulus is expected to become sensitive to the increased fraction of surface atoms and to possible surface tension effects.[96]

Some research groups have carried out mechanical measurements on individual nanowires, using different approaches, predominantly using either an AFM or a home-built system incorporated within a TEM or SEM. In 1997, the elastic strength and toughness of silicon carbide nanorods and multiwalled carbon nanotubes were studied by Wong and co-workers[97] using an AFM based technique. Poncharal *et al.* reported a method involving electrical excitation of MWNTs at their resonance frequency in situ in a TEM and simultaneously measured the induced dynamic deflection of the tube. In this method, the Young's modulus, which could be calculated from the resonant frequency and the dimensions of the wire, was found to decrease sharply with increasing diameter.[98] This method was also applied to a Kelvin probe based on nanotubes and a nanobalance able to measure in the picogram to femtogram range. Ruoff and co-workers[99] used a nanostressing stage inside a SEM and recorded the entire experiment on video, enabling realtime characterization of the deformation. In these experiments, individual MWNTs were picked up and attached onto the opposing tips of AFM cantilever probes. The idea for this experiment came from a classical macroscale tensile load experiment. With this method, a wide range of mechanical properties of a large number of nanowires can be obtained, such as the Young's modulus, the force at fracture, and the tensile strength. TEM imaging also revealed different fracture patterns such as wavelike structures, ribbon-like distortions, and radial collapses.[100] In 2005, an AFM-based technique was developed by Wang and co-workers and has the key advantage of being nondestructive toward the nanowire.[101] This technique was then developed by Hoffmann *et al.* by mounting an AFM inside the SEM.[102] The AFM tip was used to bend standing silicon nanowires until fracture. The maximum stress before fracture can be calculated from the bending of the AFM tip, and the diameter and the length of the nanowire can be measured from the SEM image correctly. A relation between strength and length was also reported, such that shorter nanowires tend to have greater fracture strength than longer ones.

In our group, a home-built system incorporated within a SEM and a commercial system for STM-TEM and AFM-TEM are built. With these powerful tools, some work on nanomechanics of nanowires has been done since 2000.

3.2.1 Reversible bending of Si_3N_4 nanowires. As early as in 2000, we observed that Si_3N_4 nanowires were obviously bent under electron beam illumination if the current density was large enough.[103] Investigations on the mechanical properties of individual Si_3N_4 nanowires were carried out by the TEM method. In Fig. 17(b), the Si_3N_4 nanowire is at its original position. As the average current density was increased, the nanowire began to bend away from the center of the beam. As shown in Fig. 17 (a), the bending angle was nearly 100° when the center of the beam was at the right upper corner marked as B. When the center of the electron beam was moved to the other side of this nanowire, the nanowire bent immediately to the opposite side [Fig. 17 (c)]. With the average current density

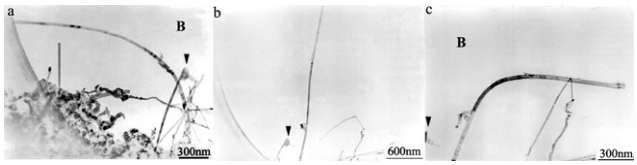

Fig. 17 Bending of Si_3N_4 nanowire: (a) bend to right, (b) at original position when the average density of the electron beam is small, and (c) bend to left. The B is marked as the center of the illumination beam (ref. 103).

decreasing to a very small value, the wirereturned to its original straight position. The results showed that, under the illumination of the electron beam, ceramic nanowires, for example Si_3N_4 nanowires, were found to be bent with good flexibility. The bending strengths of Si_3N_4 nanowires were found to be much higher than those of the corresponding bulk materials. Further studies show that the bending deflection f was proportional to the square of the beam current density J^2. The bending could not occur unless either the nanowire/nanotube or the supporting film was an insulator. We believe that the electrostatic force induced by the charge accumulation on the nanowires results in the bending of the ceramic nanowires. This work may lead to a way to calculate the elastic modulus of nanowires/nanotubes.

3.2.2 ZnO: size dependence of Young's modulus. In our group, Young's modulus of ZnO NWs with diameters ranging from 17 to 550 nm has been investigated.[104] High-quality single-crystal ZnO NWs with a large range in diameter and a uniform [0001] growth orientation are fabricated by controllable thermal evaporation mentioned above.[88]

The experiment was carried out *in-situ* in the scanning electron microscope (SEM), using the electric field induced mechanical resonance (EFIR) method. Multi-frequency resonance behaviors of ZnO nanowires in electric fields were studied experimentally and theoretically. It was identified that the resonances included two different modes: forced resonances driven by periodic transverse force and parametric resonances driven by periodic axial forces, which are shown in Fig. 18. With the good identification of the natural frequencies of nanowires, a size dependence of Young's modulus in [0001] oriented ZnO NWs with diameters ranging from 17 to 550 nm was revealed.

The measured values of the Young's modulus E of ZnO NWs are shown as a function of the diameter in Fig. 19. As shown in Fig. 19, for NWs with larger diameters D (> about 120 nm) the measured Young's modulus is slightly dependent on the diameter and tends to the value of bulk ZnO, while the D is decreasing from 120 nm to 17 nm the measured values are dramatically increasing.

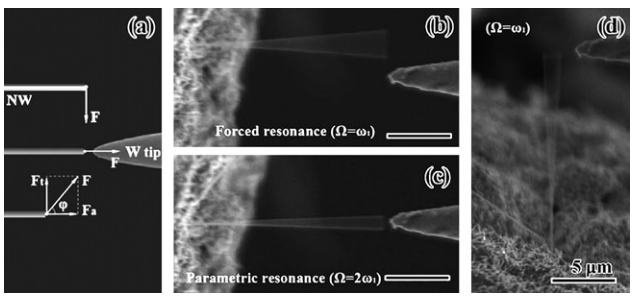

Fig. 18 Resonances of a ZnO NW in different experimental configurations. (a) (Schematic) Relative magnitude of the transverse force F_t and the axial force F_a; ϕ denotes the angle between F and the NW axis. (b) SEM micrograph for the NW located off-axis ($\phi = 90°$), the force was transverse and the NW exhibited forced resonances ($V_{ac} = 2$ V, $V_{dc} = 2$ V, $\Omega = \omega 1$). (c) SEM micrograph for the NW located on-axis with $\phi = 0°$, the force was axial and the NW exhibited parametric resonances ($V_{ac} = 2$ V, $V_{dc} = 2$ V, $\Omega = 2\omega 1$). (d) SEM micrograph of the NW perpendicular to the tip axis, the force was transverse and the NW exhibited forced resonances ($V_{ac} = 1$ V, $V_{dc} = 1$ V, $\Omega = \omega 1$) (ref.104).

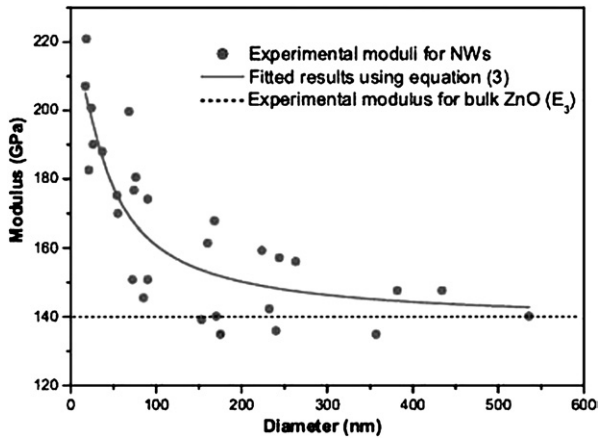

Fig. 19 Diameter dependence of effective Young's modulus in (0001) oriented ZnO nanowires for bending: (dots) experimental results, (solid line) fitted results by the core-shell composite NW model, (dashed line) modulus for bulk ZnO (E3) (ref. 104).

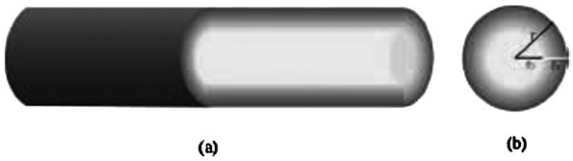

Fig. 20 (a) Schematic illustration of the core-shell composite NW model; (b) the cross section (ref. 104).

A core-shell composite NW model (Fig. 20) in terms of surface stiffening effect correlated with significant bond length contractions occurring near the {10−10} free surface (which extend several layers deep into the bulk and fade off slowly) was proposed to explore the origin of the size dependence, and it has been demonstrated that surface effects play a significant role in determining the mechanical properties of ZnO NWs. With this core-shell model for a ZnO NW, the abnormal increase of Young's modulus with decreasing wire diameter is well explained.

3.2.3 Bending strength flexibility of ZnO nanowires. A quantitative study on the fracture strain, strength, and flexibility of ZnO NWs with a large range of diameters (85–542nm) based on a in-situ SEM nanomechanical bending experiments has also been reported.[105]

High quality [0001] oriented ZnO NWs were prepared using the same method as described in ref. 88. The experimental NWs generally have cone-shaped roots, as shown in Fig. 21(a). A homemade nanomanipulator in the SEM with a sharp tungsten tip was used to deflect a ZnO NW to different levels until it was finally broken, as shown in Fig. 21(b–d). Consistent with the reported behaviors of Si_3N_4, Si, and SiC NWs and ZnO nanobelts,[106] the NWs show an elastic fracture behavior at limit strains typically between 4%–7%, without detectable plastic deformation observed, corresponding to fracture strengths close to ideal strength. The large fracture strains and thus large

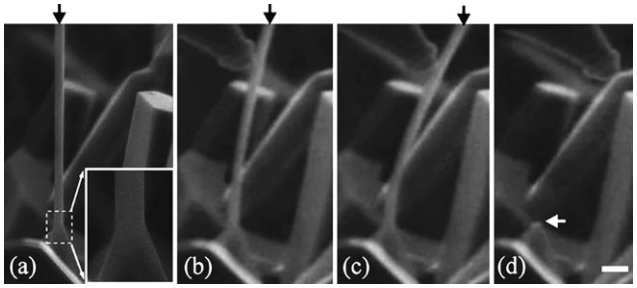

Fig. 21 (a) Low magnification image of a NW and the enlarged image of its root in the inset. (b)–(d) Selected frames of a video recording the NW subjected to different deflections indicated by black arrows in (b) and (c), and finally fractured with the fracture surface marked with a white arrow in (e). Scale bar represents 1 μm (ref. 105).

strengths are attributed to a lack of defects and flaws. The commonly observed exceptional flexibility for ceramic NWs is an exhibition of large elastic fracture strains due to a lack of defects, is geometrically related to the very small diameters, and can be determined quantitatively.

4. The application of inorganic nanowire arrays

Solar cells based on VA and SA-Si nanowire arrays

These days, the exploitation of renewable energy, especially solar energy, has become an essential measure to address present energy shortages and environmental problems. Special focus has been put on the possible applications of nanotechnology in power sources, such as ZnO nanowire based nanogenerators,[107] and Nafion™ nanowire based fuel cells.[108] Silicon-based solar cells play a dominant role in the photovoltaic (PV) market at present. Due to their novel properties, the utilization of silicon nanowires in solar cells has become an interesting topic.

Some nanowire-based solar cells have been reported,[109] but as early as 2005, a novel photovoltaic cell using oriented silicon nanowire arrays was proposed and demonstrated by our group.[110,111]

The Si NW arrays are fabricated using our metal-assisted chemical etching method. Fig. 22(a–d) show images of the as-prepared vertical aligned (VA) and slantingly aligned (SA) SiNW arrays. Compared with the VA-Si NWs, Fig. 22(c) and (d) are the planar and the cross-sectional views, respectively, of the SA-SiNW arrays, and show clearly that SiNWs produced from p-type Si(111) substrates are aligned slantingly on the surface of the silicon wafer.

It has been proved that the special structure of our SiNW array could effectively reduce the reflection loss. Optical reflectance spectra of SA-SiNW arrays, VA-SiNW arrays and polished Si wafers are shown in Fig. 22(e). The average reflectance of SA-SiNW arrays is about 5% over the range of 300–1000 nm, a little higher than that of VA-SiNW arrays (about 2.5%), but much less than that of polished Si wafer (above 20%). The very dense SiNW arrays with high aspect ratio, whether vertically or slantingly aligned, show a small optical loss of the incoming light, because most of the incoming light could be absorbed after multiple reflections in the forest of SiNW arrays. The small difference between the reflectance of SA-SiNW arrays and VA-SiNW

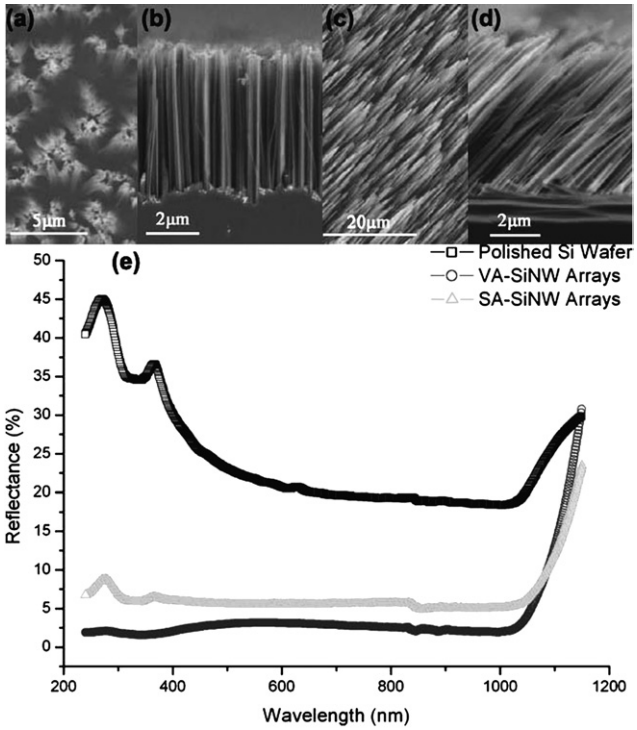

Fig. 22 (a) SEM image of surface morphology of VA-Si nanowire arrays. (b) SEM image of cross-section view of VA-Si nanowire arrays. (c) SEM image of surface morphology of SA-Si nanowire arrays. (d) SEM image of cross-section view of SA-Si nanowire arrays. (e) Reflectance spectra of VA and SA SiNW arrays and initial Si wafer (ref. 110 and 111).

arrays is probably due to the reflection of light from the upper parts of the slanting arrays.

Utilizing the excellent anti-reflection characteristic of large-area SiNW arrays over a wide spectral bandwidth between 1200–300 nm, we have designed and manufactured a new type of solar cell based on VA-SiNW arrays.[110] A power conversion efficiency of 9.32%, open circuit voltage of 548.5 mV, short circuit current of 26.06 mA and fill factor of 0.6512 were obtained, as illustrated in Fig. 23(a).

The performance of our newly fabricated Si(111)-based SA-SiNW array solar cells has been improved remarkably, with the highest values of a power conversion efficiency of 11.37%, open circuit voltage of 580.25 mV, short circuit current of 27.14 mA and fill factor of 0.7222. The test result can be seen in Fig. 23(b). Compared to the VA-nanowire based solar cells, the improved device performance is attributed to a combination of the excellent anti-reflection properties of the arrays and the decreasing series resistance of the cell from the special slantingly aligned structure.

In order to achieve a high power conversion efficiency of SiNW-based solar cells, it is necessary to reduce charge recombination, which decreases the external quantum efficiency (EQE) and the fill factor. Highly stable SiNW density and charge collection efficiency of electrode are also especially expected.

Our present results suggest the potential application of SiNW in PV technology and also offer new opportunities in solar PV technology.

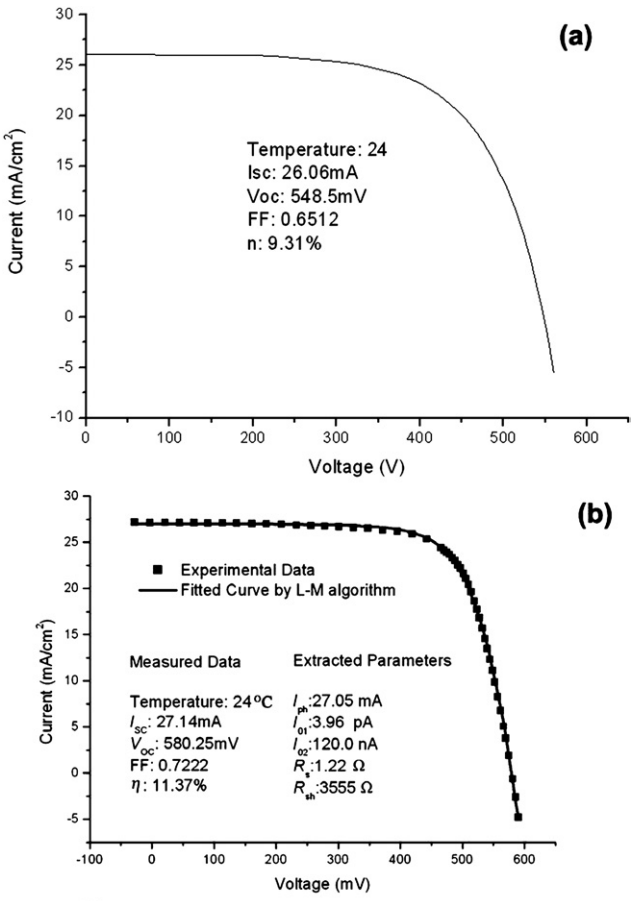

Fig. 23 I-V curves for different types of solar cells: (a) Current–voltage (I/V) characteristics of a photovoltaic device based on VA-SiNW arrays prepared on a monocrystalline Si substrate. (b) Current–voltage (I/V) characteristics of our as-fabricated SA-SiNW array solar cell with highest performance (ref. 110 and 111).

5. Outlook

In the last decade, there have been intense activities in preparing nanowires with favourable quantities. Obviously, nanowires of much more inorganic materials will be prepared in the future with new methods. However, the mechanisms of the growth of nanowires in most cases are not clearly known since most of the nanowires are formed under a non-equilibrium state and controlled by kinetic processes. To have a better understanding of this, there is a need for theoretical and computational effort, which can also provide predictions on the certain growth of some novel structures. Even more efforts are needed for more complicated systems involving new structural morphologies and new processes.

Furthermore, with the development of those in-situ nanomanipulate systems, the investigations can be conducted now on the electrical, mechanical, magnetic, optical and other properties of nanowires. Based on these studies, nanowires will be possibly exploited as device elements in future architectures in nanosystems.

6. Summary

In the last decade, much effort has been devoted to study those nanowires which attract tremendous interest due to their novel size- and dimensionality-dependent physical properties and their potential applications in nanoscale functional electronics and photonics.

In this feature article, a review of our contributions in the 1D inorganic nanowires field is presented. Several synthesis methods have been developed in our group, including template assisted chemical deposition, CVD, electrospinning, *etc*., especially the metal assisted chemical etching and catalytic templated etching processes, which provide a novel access to fabricate Si nanowire arrays (structure) and attract much attention in the nano-science and technology field. *Via* these methods, various nanowires, such as Si nanowires, and nanostructured metallic nanowires (Ag, Ni, Pt, Cu, Fe *etc*.), oxide and nitride nanowires (ZnO, SiO_2, AlN, Ga_2O_3, GaN, *etc*.), heterojunction nanowires (Ni/MWCNT/a-CNT, Ag/a-CNT, Ag/Si and Pt_6Si_5/Si), *etc*., have been prepared.

With thorough structure characterization of these nanowires, some unique phenomena are observed due to the size effect of nanowires. 4H-structured Ag (which is absent in bulk Ag) nanowires coexist with FCC-structured AgNWs with diameters ranging between 8–100 nm, because of the favorable surface energy. FCC and HCP Ni are also revealed in single crystal Ni nanowire arrays.

In addition, some important properties of these nanowires, including electronic, mechanical and magnetic properties, are thoroughly investigated.

It was revealed that both the 4H- and the FCC-AgNWs are metallic conductors, with comparable average resistivity, one order of magnitude higher than that of bulk FCC-Ag, indicating a bright future in applications as interconnecting elements. The contacts between the a-CNTs and the metal nanowires are proved to be ohmic. This finding has universal significance and offers a wide opportunity for designing large-scale interconnections among nanowires.

An extraordinary mechanical property of ZnO was investigated in our group: a size dependence of Young's modulus in [0001] oriented ZnO NWs with diameters ranging from 17 to 550 nm was revealed, and surface effects are thought to play a significant role in determining the mechanical properties of ZnO NWs according to our core-shell model.

For magnetic properties, single crystal FCC-Ni nanowires are found to have good magnetic properties, and may have potential applications in perpendicular magnetic recording.

Inspired by the excellent anti-reflection properties of Si nanowire arrays, Si nanowire based solar cells have been developed. It shows the potential application of SiNW in photovoltaic technology and may also offer new opportunities in solar photovoltaic technology.

Acknowledgements

This work is financially supported by National 973 Project of China, Chinese National Nature Science Foundation. The authors thank Jun Luo, Kuiqing Peng, Changqiang Chen, Yingjiu Zhang, Hui Fang, Feng Tian, Zhipeng Huang, Yousheng Zhang, Lu Zhang, Fan Zhang, Jing Chen, Yu Shi and Zhixiang Luo for their discussions and providing those original data which are used in this article.

References

1 R. Notzel and K. H. Ploog, *Adv. Mater*, 1993, **5**, 22; H. Weller, *Adv. Mater.*, 1993, **5**, 88; B. Wiley, Y. G. Sun and J. Y. Chen, *MRS Bulleti*, 2005, **30**, 356; Y. J. Xiong and Y. N. Xia, *Adv. Mater.*, 2007, **19**, 3385.

2 M. Nirmal and L. Brus, *Acc. Chem. Res.*, 1999, **32**, 407; V. I. Klimov, A. A. Mikhailovsky, S. Xu, A. Malko, J. A. Hollingsworth, C. A. Leatherdale, H. J. Eisler and M. G. Bawendi, *Science*, 2000, **314**, 290; D. L. Klein, R. Roth, A. K. L. Lim, A. P. Alivisatos and P. L. McEuen, *Nature*, 1997, **389**, 699; H. Pettersson, L. Baath, N. Carlsson, W. Seifert and L. Samuelson, *Appl. Phys. Lett.*, 2001, **79**, 78; A. N. Shipway, E. Katz and I. Willner, *Chem. Phys. Chem.*, 2000, **1**, 18; A. J. Phillips, *J. Appl. Phys.*, 2002, **91**, 4590; A. S. Coe, W. L. Woo, M. Bawendi and V. Bulovic, *Nature*, 2002, **420**, 800; A. V. L. Colvin, M. C. Schlamp and A. P. Alivisatos, *Nature*, 1994, **370**, 354.

3 D. T. Colbert, J. Zhang, S. M. McClure, P. Nikolaev, Z. Chen, J. H. Hafner, D. W. Owens, P. G. Kotula, C. B. Carter, J. H. Weaver, A. G. Rinzler and R. E. Smalley, *Science*, 1994, **266**, 1218.

4 A. M. Morales and C. M. Lieber, *Science*, 1998, **279**, 208.

5 Y. Peng, H. L. Zhang, S. L. Pan and H. L. Li, *J. Appl. Phys*, 2000, **87**, 7405.

6 Y. Lei, L. D. Zhang, G. W. Meng, G. H. Li, X. Y. Zhang, C. H. Liang, W. Chen and S. X. Wang, *Appl. Phys. Lett.*, 2001, **78**, 1125.

7 D. N. Davydov, P. A. Sattari, D. AlMawlawi, A. Osika, T. L. Haslett and M. Moskovits, *J. Appl. Phys.*, 1999, **86**, 3983.

8 H. Wu, R. Zhang, X. Liu, D. Lin and W. Pan, *Chem. Mater.*, 2007, **19**, 3506; H. Wu, D. Lin and W. Pan, *Appl. Phys. Lett.*, 2006, **89**, 133125; H. Wu, D. Lin, R. Zhang and W. Pan, *J. Am. Ceram. Soc.*, 2008, **91**, 656.

9 S. Iijima, *Nature*, 1991, **354**, 56.

10 D. P. Yu, Z. G. Bai, Y. Ding, Q. L. Hang, H. Z. Zhang, J. J. Wong, Y. H. Zou, W. Qian, Q. C. Xiong, H. T. Zhou and S. Q. Feng, *Appl. Phys. Lett.*, 1998, **72**, 3458.

11 G. Audoit, E. N. Mhuircheartaigh, S. M. Lipson, M. A. Morris, W. J. Blau and J. D. Holmes, *J. Mater. Chem.*, 2005, **15**, 4809; G. Audoit, J. S. Kulkarni, M. A. Morris and J. D. Holmes, *J. Mater. Chem.*, 2007, **17**, 1608.

12 C. J. Otten, O. R. Louire, M. F. Yu, J. M. Couley, M. J. Dyer, R. S. Ruoff and W. E. Buhro, *J. Am. Chem. Soc.*, 2002, **124**, 4564.

13 D. P. Yu, Q. L. Hang, Y. Ding, H. Z. Zhang, Z. G. Bai, J. J. Wang, Y. H. Zou, W. Qian, G. C. Xiong and S. Q. Feng, *Appl. Phys. Lett.*, 1998, **73**, 3076.

14 G. Gundiah, A. Govindaraj and C. N. R. Rao, *Chem. Phys. Lett.*, 2002, **351**, 189; B. Cheng and E. T. Samulski, *J. Mater. Chem.*, 2001, **11**, 2901.

15 Y. D. Yin, G. T. Zhang and Y. N. Xia, *Adv. Funct. Mater.*, 2002, **12**, 293.

16 Y. X. Zhang, G. H. Li, Y. X. Jin, Y. Zhang, J. Zhang and L. D. Zhang, *Chem. Phys. Lett.*, 2002, **365**, 300; H. Imai, Y. Takei, K. Shimizu, M. Matsuda and H. Hirashima, *J. Mater. Chem.*, 1999, **9**, 2971; C. A. Grimes, *J. Mater. Chem.*, 2007, **17**, 1451; J. Cao, J. Z. Sun and H. Y. Li, *J. Mater. Chem.*, 2004, **14**, 1203; X. S. Peng and A. C. Chen, *J. Mater. Chem.*, 2004, **14**, 2542; S. S. Kim, C. Chun, J. C. Hong and D. Y. Kim, *J. Mater. Chem.*, 2006, **16**, 370.

17 T. He and J. N. Yao, *J. Mater. Chem.*, 2007, **17**, 4547.

18 X. F. Duan and C. M. Lieber, *J. Am. Chem. Soc.*, 2000, **122**, 188; S. M. Zhou, Y. S. Feng and L. D. Zhang, *Chem. Phys. Lett.*, 2003, **369**, 610.

19 J. Liu, X. Z. Zhang, Y. J. Zhang, R. R. He and J. Zhu, *J. Mater. Res.*, 2001, **16**, 3133.

20 J. Wei, B. Jiang, Y. Li, C. Xu, D. Wu and B. Wei, *J. Mater. Chem.*, 2002, **12**, 3121; K. Sardar, M. Dan, B. Schwenzer and C. N. R. Rao, *J. Mater. Chem.*, 2005, **15**, 2175.

21 K. Sardar, F. L. Deepak, A. Govindaraj, M. M. Seikh and C. N. R. Rao, *Small*, 2005, **1**, 91.

22 H. Zhang, Q. Zhang, J. Tang and L. C. Qin, *J. Am. Chem. Soc.*, 2005, **127**, 8002.

23 H. Zhang, Q. Zhang, J. Tang and L. C. Qin, *J. Am. Chem. Soc.*, 2005, **127**, 2862.

24 H. J. Dai, E. W. Wong, Y. Z. Lu, S. S. Fan and C. M. Lieber, *Nature*, 1995, **375**, 769; C. C. Tang, Y. Bando, T. Sato and K. Kurashima, *J. Mater. Chem.*, 2002, **12**, 1910; Y. Q. Zhu, W. B. Hu, W. K. Hsu, M. Terrones, N. Grobert, J. P. Hare, H. W. Kroto, D. R. M. Walton and H. Terrones, *J. Mater. Chem.*, 1999, **9**, 3173.

25 D. S. Xu, Y. J. Xu, D. P. Chen, G. L. Guo, L. L. Cui and Y. Q. Tang, *Adv. Mater.*, 2000, **12**, 520; M. Chen, Y. Xie, J. Lu, Y. Xiong, S. Zhang, Y. Qian and X. Liu, *J. Mater. Chem.*, 2002, **12**, 748; S. H. Yu, J. Yang, Z. H. Han, Y. Zhou, R. Y. Yang, Y. T. Qian and Y. H. Zhang, *J. Mater. Chem.*, 1999, **9**, 1283; Y. Wada, H. Kuramoto, J. Anand, T. Kitamura, T. Sakata, H. Mori and S. Yanagida, *J. Mater. Chem.*, 2001, **11**, 1936; Y. C. Li, X. H. Li, C. H. Yang and Y. F. Li, *J. Mater. Chem.*, 2003, **13**, 2641; J. Cao, J. Z. Sun and H. Y. Li, *J. Mater. Chem.*, 2004, **14**, 1203; M. Chen, Y. Xie, Z. Qiao, Z. Zhu and Y. Qian, *J. Mater. Chem.*, 2000, **10**, 329; Z. H. Dai, J. Zhang, J. C. Bao, X. H. Huang and X. Y. Mo, *J. Mater. Chem.*, 2007, **17**, 1087.

26 D. J. Pena, J. K. N. Mbindyo, A. J. Carado, T. E. Mallouk, C. D. Keating, B. Razavi and T. S. Mayer, *J. Phys. Chem. B*, 2002, **106**, 7458; Q. Yang, K. B. Tang, C. R. Wang, Y. T. Qian and S. Y. Zhan, *J Phys. Chem. B*, 2002, **106**, 9227; S. Sapra, A. L. Rogach and J. Feldmann, *J. Mater. Chem.*, 2006, **16**, 3391.

27 Q. Yang, K. Tang, C. Wang, Y. Qian and S. Zhang, *J Phys. Chem. B*, 2002, **106**, 9227; W. I. Park, H. S. Kim, S. Y. Jang, J. Park, S. Y. Bae, M. Jung, H. Lee and J. Kim, *J. Mater. Chem.*, 2008, **18**, 875; M. W. DeGroot, N. J. Taylor and J. F. Corrigan, *J. Mater. Chem.*, 2004, **14**, 654.

28 M. S. Mo, M. W. Shao, H. M. Hu, L. Yang, W. C. Yu and Y. T. Qian, *J. Cryst. Growth.*, 2002, **244**, 364; F. Gao, Q. Lu, X. Liu, Y. Yan and D. Zhao, *Nano. Lett.*, 2001, **1**, 743; D. B. Yu, D. B. Wang, Z. Y. Meng, J. Lu and Y. T. Qian, *J. Mater. Chem.*, 2002, **12**, 403; M. Afzaal and P. O'Brien, *J. Mater. Chem.*, 2006, **16**, 1113.

29 W. Wang, Y. Geng, Y. Qian, M. Ji and X. Liu, *Adv. Mater.*, 1998, **10**, 1479; M. Chen, Y. Xie, J. C. Lu, Y. J. Zhu and Y. T. Qian, *J. Mater. Chem.*, 2001, **11**, 518.

30 C. Y. Wu, S. H. Yu, S. Chen, G. N. Liu and B. H. Liu, *J. Mater. Chem.*, 2006, **16**, 3326.

31 A. Govindaraj, F. L. Deepak, N. A. Gunari and CNR Rao, *Israel J. Chem.*, 2001, **41**, 23; H. Li, Y. Zhu, S. Avivi, O. Palchick, J. Xiong, Y. Koltypin, V. Palchick and A. Gedanken, *J. Mater. Chem.*, 2002, **12**, 3723; Y. Zhang, Z. P. Qiao and X. M. Chen, *J. Mater. Chem.*, 2002, **12**, 2747.

32 B. Gates, B. Mayers, Y. Wu, Y. Sun, B. Cattle, P. Yang and Y. Xia, *Adv. Funct. Mater.*, 2002, **12**, 679; Y. J. Glanville, D. G. Narehood, P. E. Sokol, A. Amma and T. Mallouk, *J. Mater. Chem.*, 2002, **12**, 2433.

33 S. Hofmann, C. Ducati and J. Robertson, *Adv. Mater.*, 2002, **14**, 1821.

34 M. Nath and C. N. R. Rao, *J. Am. Chem. Soc.*, 2001, **123**, 4841; C. Schuffenhauer, R. Popovitz-Biro and R. Tenne, *J. Mater. Chem.*, 2002, **12**, 1587; Y. Yang, M. Nogami, J. Shi, H. Chen, Y. Liu and S. Qian, *J. Mater. Chem.*, 2003, **13**, 3026.

35 J. J. Urban, W. S. Yun and H. Park, *J. Am. Chem. Soc.*, 2002, **124**, 1186.

36 G. H. Du, Q. Chen, P. D. Han, Y. Yu and L. M. Peng, *Phys. Rev. B*, 2003, **67**, 035323.

37 B. D. Busbee, S. O. Obare and C. J. Murphy, *Adv. Mater.*, 2003, **15**, 414; X. Y. Zhang, L. D. Zhang, Y. Lei, L. X. Zhao and Y. Q. Mao, *J. Mater. Chem.*, 2001, **11**, 1732; A. I. Bhatt, A. M. Mechler, L. L. Martin and A. M. Bond, *J. Mater. Chem.*, 2007, **17**, 2241; S. H. Liu, J. B. H. Tok and Z. N. Bao, *Nano Lett.*, 2005, **5**, 1071.

38 C. Y. Wang, M. Chen, G. M. Zhu and Z. G. Lin, *J. Colloid Interface Sci.*, 2001, **243**, 362; M. H. Huang, A. Choudrey and P. D. Yang, *Chem. Commun.*, 2000, 1063.

39 S. Sun, D. Yang, G. Zhang, E. Sacher and J. Dodelet, *J. Chem. Mater.*, 2007, **19**, 6376; Y. Song, R. M. Garcia, R. M. Dorin, H. R. Wang, Y. Qiu, E. N. Coker, W. A. Steen, J. E. Miller and J. A. Shelnutt, *Nano. Lett.*, 2007, **7**, 3650; X. M. Yan, S. Kwon, A. M. Contreras, J. Bokor and G. A. Somorjai, *Nano Lett.*, 2005, **5**, 745.

40 T. Gao, G. Meng, J. Zhang, C. Liang, J. Fan and L. Zhang, *Appl. Phys. A*, 2001, **73**, 251.

41 J. Wang, *J. Mater. Chem.*, 2008, **18**, 4017.

42 C. F. Pan, L. Zhang, J. Zhu, J. Luo, Z. D. Cheng and C. Wang, *Nanotechnology*, 2007, **18**, 015302L. Zhang, C. F. Pan, J. Zhu and C. Wang, *Nanotechnology*, 2005, **16**, 2242; L. Huang, Z. Wang, H. Wang, X. Cheng, A. Mitra and Y. Yan, *J. Mater. Chem.*, 2002, **12**, 388; J. C. Hulteen and C. R. Martin, *J. Mater. Chem.*, 1997, **7**, 1075; J. Kameoka, D. Czaplewski, H. Liu and H. G. Craighead, *J. Mater. Chem.*, 2004, **14**, 1503; J. J. Chiu, C. C. Kei, T. P. Perng and W. S. Wang, *Adv. Mater.*, 2003, **15**, 1361.

43 Q. Xu, L. Zhang and J. Zhu, *J. Phys. Chem. B*, 2003, **107**, 8294; X. F. Duan and C. M. Lieber, *Adv. Mater.*, 2000, **12**, 298.

44 W. Shi, Y. Zheng, N. Wang, C. S. Lee and S. T. Lee, *Adv. Mater.*, 2001, **13**, 591; H. Yu and W. E. Buhro, *Adv. Mater.*, 2003, **15**, 416.

45 X. Duan, Y. Huang, Y. Cui, J. Wang and C. M. Lieber, *Nature*, 2001, **409**, 66; M. S. Gudiksen, J. Wang and C. M. Lieber, *J. Phys. Chem. B*, 2002, **106**, 4036; M. S. Gudiksen, J. Wang and C. M. Lieber, *J. Phys. Chem. B*, 2001, **105**, 4062; P. Yan, Y. Xie, W. Z. Wang, F. Y. Liu and Y. T. Qian, *J. Mater. Chem.*, 1999, **9**, 1831.

46 M. S. Gudiksen and C. M. Lieber, *J. Am. Chem. Soc.*, 2000, **122**, 8801; W. S. Shi, Y. F. Zheng, N. Wang, C. S. Lee and S. T. Lee, *J Vac Sci Technol B*, 2001, **19**, 1115; H. W. Seo, S. Y. Bae, J. Park, H. Yuang and S. Kim, *Chem. Commun.*, 2002, 2564.

47 Z. W. Pan, Z. R. Dai and Z. L. Wang, *Science*, 2001, **291**, 1947.

48 J. Westwater, D. P. Gosain, S. Tomiya, S. Usui and H. Ruda, *J. Vac. Sci. Technol. B*, 1997, **15**, 554; D. P. Yu, Z. G. Bai, Y. Ding, Q. L. Hang, H. Z. Zhang, J. J. Wang, Y. H. Zou, W. Qian, G. C. Xiong, H. T. Zhou and S. Q. Feng, *Appl. Phys. Lett.*, 1998, **72**, 3458; J. D. Holmes, K. P. Johnston, R. C. Doty and B. A. Korgel, *Science*, 2000, **287**, 1471; Lih J. Chen, *J. Mater. Chem.*, 2007, **17**, 4639.

49 Y. Wang, V. Schmidt, S. Senz and U. Goesele, *Nature Nanotechnology*, **1**, 186; B. Fuhrmann, S. Leipner Hartmut, Hans-Reiner Hoeche, L. Schubert, P. Werner and U. Goesele, *Nano Lett.*, 2005, **5**, 2524.

50 Y. Li, F. Qian, J. Xiang and C. M. Lieber, *Mater. Today*, 2006, **9**(10), 18; Y. Wu, J. Xiang, C. Yang, W. Lu and C. M. Lieber, *Nature*, 2004, **430**, 61; W. M. Weber, L. Geelhaar, A. P. Graham, E. Unger, G. S. Duesberg, M. Liebau, W. Pamler, C. Cheze, H. Riechert, P. Lugli and F. Kreupl, *Nano Lett.*, 2006, **6**, 2660; K. C. Lu, K. N. Tu, W. W. Wu, L. J. Chen, B. Y. Yoo and N. V. Myung, *Appl. Phys. Lett*, 2007, **90**, 253111.

51 X. Fang, Y. Bando, C. Ye, G. Shen, U. K. Gautam, C. Tang and D. Golberg, *Chem. Commun.*, 2007, 4093.

52 N. Wang, Y. H. Tang, Y. F. Zhang, C. S. Lee, I. Bello and S. T. Lee, *Chem. Phys. Lett.*, 1999, **299**, 237.

53 Y. Cui, L. J. Lauhon, M. S. Gudiksen, J. F. Wang and C. M. Lieber, *Appl. Phys. Lett.*, 2001, **78**, 2214.

54 R. S. Wagner and W. C. Ellis, *Appl. Phys. Lett.*, 1964, **4**, 89.

55 Q. Gu, H. Dang, J. Cao, J. Zhao and S. Fan, *Appl. Phys. Lett.*, 2000, **76**, 3020.

56 J. D. Holmes, K. P. Johnston, R. C. Doty and B. A. Korgel, *Science*, 2000, **287**, 1471.

57 Y. Wang, V. Schmidt, S. Senz and U. Goesele, *Nature Nanotechnology*, 2006, **1**, 186; T. I. Kamins, R. S. Williams, Y. Chen, Y. L. Chang and Y. A. Chang, *Appl. Phys. Lett.*, 2000, **76**, 562.

58 R. Q. Zhang, Y. Lifshitz and S. T. Lee, *Adv. Mater.*, 2003, **15**, 635; N. Wang, Y. F. Zhang, Y. H. Tang, C. S. Lee and S. T. Lee, *Appl. Phys. Lett.*, 1998, **73**, 3902; D. D. D. Ma, C. S. Lee, F. C. K. Au, S. Y. Tong and S. T. Lee, *Science*, 2003, **299**, 1874.

59 K. Q. Peng, Y. J. Yan, S. P. Gao and J. Zhu, *Adv. Mater.*, 2002, **14**, 1164; K. Q. Peng, Y. J. Yan, S. P. Gao and J. Zhu, *Adv. Funct. Mater.*, 2003, **13**, 127; K. Q. Peng and J. Zhu, *J Electroanal. Chem.*, 2003, **558**, 35; K. Q. Peng, Z. P. Huang and J. Zhu, *Adv. Mater.*, 2004, **16**, 73; K. Q. Peng and J. Zhu, *Electrochim. Acta*, 2004, **49**, 2563; K. Q. Peng, H. Fang, J. J. Hu, Y. Wu, J. Zhu, Y. J. Yan and S. Lee, *Chem-Eur. J.*, 2006, **12**, 7942; K. Q. Peng, J. J. Hu, Y. J. Yan, Y. Wu, H. Fang, Y. Xu, S. T. Lee and J. Zhu, *Adv. Funct. Mater.*, 2006, **16**, 387.

60 T. Qiu, X. L. Wu, G. G. Siu and P. K. Chu, *J. Electron. Mater.*, 2006, **35**, 1879; T. Qiu, X. L. Wu, X. Yang, G. S. Huang and Z. Y. Zhang, *Appl. Phys. Lett.*, 2004, **84**, 3867.

61 K. Q. Peng, J. J. Hu, Y. J. Yan, Y. Wu, H. Fang, Y. Xu, S. T. Lee and J. Zhu, *Adv. Funct. Mater.*, 2006, **16**, 387; K. Q. Peng, H. Fang, J. J. Hu, Y. Wu, J. Zhu, Y. J. Yan and S. T. Lee, *Chem. Eur. J.*, 2006, **12**, 7942.

62 H. Fang, Y. Wu, J. H. Zhao and J. Zhu, *Nanotechnology*, 2006, **17**, 3768.

63 Z. P. Huang, H. Fang and J. Zhu, *Adv. Mater.*, 2007, **19**, 744.

64 A. I. Hochbaum, R. K. Chen, R. D. Delgado, W. J. Liang, E. C. Garnett, M. Najarian, A. Majumdar and P. D. Yang, *Nature*, 2008, **451**, 163.

65 C. R. Martin, *Science*, 1994, **266**, 1961; D. Almawlawi, C. Z. Liu and M. Moskovits, *J. Mater. Res.*, 1994, **9**, 1014; M. Zheng, L. Zhang, X. Zhang, J. Zhang and G. Li, *Chem. Phys. Lett*, 2001, **334**, 298.

66 F. Zhang, X. H. Liu, C. F. Pan and J. Zhu, *Nanotechnology*, 2007, **18**, 345302.

67 L. Zhang, X. Zhang, C. F. Pan and J. Zhu, *Science in China Series E: Technological Sciences*, 2008, **51**, in press.

68 H. Masuda, G. Hasegwa and S. Ono, *J. Electrochem. Soc.*, 1997, **144**, L127; X. Zhang, Thesis, Tsinghua University, 2003; H. Masuda, K. Yada and A. Osaka, *Japan. J. Appl. Phys.*, 1998, **37**, L1340.

69 N. R. Jana, L. Gearheart and C. J. Murphy, *Chem. Commun.*, 2001, 617; X. Jiang, Y. Xie, J. Lu, L. Zhu, W. He and Y. Qian, *J. Mater. Chem.*, 2001, **11**, 1775; Y. Sun and Y. Xia, *Adv. Mater.*, 2002, **14**, 833.

70 G. Sauer, G. Brehm, S. Schneider, K. Nielsch, R. B. Wehrspohn, J. Choi, H. Hofmeister and U. Gosele, *J. Appl. Phys.*, 2002, **91**, 3243; J. Choi, G. Sauer, K. Nielsch, R. B. Wehrspohn and U. Gosele, *Chem. Mater*, 2003, **15**, 776.

71 X. H. Liu, J. Luo and J. Zhu, *Nano Lett.*, 2006, **6**, 408; X. H. Liu, R. Huang and J. Zhu, *Chem. Mater.*, 2008, **20**, 192.

72 H. Zeng, R. S. Skomski, L. Menon, Y. Liu, S. Bandopadhyay and D. J. Sellmyer, *Phys. Rev. B.*, 2002, **65**, 1.

73 F. Tian, J. Zhu, D. Wei and Y. T. Shen, *J Phys. Chem. B*, 2005, **109**, 14852; F. Tian, J. Zhu and D. Wei, *J Phys. Chem. C*, 2007, **111**, 12669; F. Tian, J. Zhu and D. Wei, *J Phys. Chem. C*, 2007, **111**, 6994; F. Tian, J. Chen, J. Zhu and D. Wei, *J. Appl. Phys.*, 2008, **103**, 013901.

74 J. T. Hu, M. Ouyang, P. D. Yang and C. M. Lieber, *Nature*, 1999, **399**, 48.

75 Y. Zhang, T. Ichihashi, E. Landree, F. Nihey and S. Iijima, *Science*, 1999, **285**, 1719.

76 Y. Y. Wu, R. Fan and P. D. Yang, *Nano. Lett.*, 2002, **2**, 83.

77 M. T. Björk, B. J. Ohlsson, T. Sass, A. I. Persson, C. Thelander, M. H. Magnusson, K. Deppert, L. R. Wallenberg and L. Samuelson, *Nano. Lett.*, 2002, **2**, 87.

78 M. S. Gudiksen, L. J. Lauhon, J. Wang, D. C. Smith and C. M. Lieber, *Nature*, 2002, **415**, 617.

79 N. I. Kovtyukhova, B. R. Martin, J. K. N. Mbindyo, P. A. Smith, B. Razavi, T. S. Mayer and T. E. Mallouk, *J. Phys. Chem. B*, 2001, **105**, 8762; N. I. Kovtyukhova, B. R. Martin, J. K. N. Mbindyo, T. E. Mallouk, M. Cabassi and T. S. Mayer, *Mat. Sci. Eng. C*, 2002, **19**, 255.

80 W. I. Park, G. C. Yi, J. W. Kim and S. M. Park, *Appl. Phys. Lett.*, 2003, **82**, 4358.

81 D. J. Pena, J. K. N. Mbindyo, A. J. Carado, T. E. Mallouk, C. D. Keating, B. Razavi and T. S. Mayer, *J. Phys. Chem. B*, 2002, **106**, 7458.

82 Y. Wu, J. Xiang, C. Yang, W. Lu and C. M. Liber, *Nature*, 2004, **430**, 61.

83 J. H. Zhan, Y. Bando, J. Q. Hu, Z. W. Liu, L. W. Yin and D. Golberg, *Angew. Chem. Int. Ed.*, 2005, **44**, 2140.

84 J. Luo, Z. P. Huang, Y. G. Zhao, L. Zhang and J. Zhu, *Adv. Mater.*, 2004, **16**, 1512; J. Luo, L. Zhang, Y. J. Zhang and J. Zhu, *Adv. Mater.*, 2002, **14**, 1413; J. Luo and J. Zhu, *Nanotechnology*, 2006, **17**, S262.

85 J. Luo and J. Zhu, *Science*, 2004, **303**, 766c.

86 Y. J. Zhang, N. L. Wang, S. P. Gao, R. R. He, S. Miao, J. Liu, J. Zhu and X. Zhang, *Chem. Mater.*, 2002, **14**, 3564; Y. J. Zhang, H. Ago, J. Liu, M. Yumura, K. Uchida, S. Ohshima, S. Iijima, J. Zhu and X. Z. Zhang, *J Cryst. Growth*, 2004, **264**, 363; Y. J. Zhang and J. Zhu, *Micron*, 2002, **33**, 523; Y. J. Zhang, N. L. Wang, R. R. He, X. H. Chen and J. Zhu, *Solid State Commun.*, 2001, **118**, 595; Y. J. Zhang, J. Liu, R. R. He, Q. Zhang, X. Zhang and J. Zhu, *Chem. Phys. Lett.*, 2002, **360**, 579; Y. J. Zhang, J. Zhu, Q. Zhang, Y. J. Yan, N. L. Wang and X. Z. Zhang, *Chem. Phys. Lett.*, 2000,

317, 504; Y. J. Zhang, J. Liu, R. R. He, Q. Zhang, X. Z. Zhang and J. Zhu, *Chem. Mater.*, 2001, **13**, 3899; Y. J. Zhang, N. L. Wang, R. R. He, J. Liu, X. Z. Zhang and J. Zhu, *J Cryst. Growth*, 2001, **233**, 803; Y. J. Zhang, Q. Zhang, N. L. Wang, Y. J. Yan, H. H. Zhou and J. Zhu, *J Cryst. Growth*, 2001, **226**, 185.

87 X. D. Wang, J. H. Song and Z. L. Wang, *J. Mater. Chem.*, 2007, **17**, 711; P. D. Yang, H. Q. Yan, S. Mao, R. Russo, J. Johnson, R. Saykally, N. Morris, J. Pham, R. He and H. J. Choi, *Adv. Funct. Mater.*, 2002, **12**, 323; L. W. Yin, M. S. Li, Y. Bando, D. Golberg, X. L. Yuan and T. Sekiguchi, *Adv. Funct. Mater.*, 2007, **17**, 270; Q. X. Zhao, P. Klason and M. Willander, *Appl. Phys. A: Mater. Sci. Process.*, 2007, **88**, 27; B. C. Cheng, Y. H. Xiao, G. S. Wu and L. D. Zhang, *Adv. Funct. Mater.*, 2004, **14**, 913; J. W. Zhao, C. H. Ye, X. S. Fang, L. R. Qin and L. D. Zhang, *Cryst. Growth Des.*, 2006, **6**, 2643; K. Zou, S. M. Zhou, X. H. Zhang, X. Y. Qi and X. F. Duan, *J. Nanosci. Nanotechnol.*, 2006, **6**, 2200.

88 Y. S. Zhang, L. S. Wang, X. H. Liu, Y. J. Yan, C. Q. Chen and J. Zhu, *J Phys. Chem. B*, 2005, **109**, 13091.

89 B. Bhushan, 2005, *Springer handbook of nanotechnology* (Berlin, Heidelberg: Springer).

90 P. C. Chang, C. J. Chien, D. Sitchtenoth, C. Ronning and J. G. Lu, *Appl. Phys. Lett.*, 2007, **90**, 113101.

91 Y. Cui, Z. Zhong, D. Wang, W. U. Wang and C. M. Lieber, *Nano Lett.*, 2003, **3**, 149.

92 H. Haick, P. T. Hurley, A. I. Hochbaum, P. Yang and N. S. Lewis, *J. Am. Chem. Soc.*, 2006, **128**, 8990.

93 A. Motayed et al., *Appl. Phys. Lett.*, 2007, **90**, 043104.

94 X. H. Liu, J. Zhu, C. H. Jin, L. M. Peng, D. M. Tang and H. M. Cheng, *Nanotechnology*, 2008, **19**, 085711.

95 J. Luo, Y. J. Xing, J. Zhu, D. P. Yu, Y. G. Zhao, L. Zhang, H. Fang, Z. P. Huang and J. Xu, *Adv. Funct. Mater.*, 2006, **16**, 1081; J. Luo, J. Zhu, Z. P. Huang and L. Zhang, *Appl. Phys. Lett.*, 2007, **90**, 033114.

96 R. C. Cammarata, *Phys. Rev. Lett.*, 1989, **62**, 2005.

97 W. Eric and P. E. Wong, *Science*, 1997, **277**, 1971.

98 P. Poncharal, D. Ugarte and W. A. de Heer, *Science*, 1999, **283**, 1513.

99 M. F. Yu, M. J. Dyer, K. Moloni, T. F. Kelly and R. S. Ruoff, *Science*, 2000, **287**, 637.

100 R. S. Ruoff, D. C. Lorent, S. Subramani and B. Chan, *Nature*, 1993, **364**, 514.

101 J. Song, E. Riedo and Z. L. Wang, *Nano Lett.*, 2005, **5**, 1954.

102 S. Hoffmann, B. Moser, J. Michler, S. H. Christiansen, V. Schmidt, S. Senz, P. Werner, U. Gosele and C. Ballif, *Nano Lett.*, 2006, **6**, 622.

103 Y. J. Zhang, N. L. Wang, R. R. He, Q. Zhang, J. Zhu and Y. J. Yan, *J Mater. Res*, 2000, **15**, 1048.

104 C. Q. Chen, Y. Shi, Y. S. Zhang, J. Zhu and Y. J. Yan, *Phys. Rev. Lett.*, 2006, **96**, 075505; Y. Shi, C. Q. Chen, Y. S. Zhang, J. Zhu and Y. J. Yan, *Nanotechnology*, 2007, **18**, 075709.

105 C. Q. Chen and J. Zhu, *Appl. Phys. Lett.*, 2007, **90**, 043105.

106 E. W. Wong, P. E. Sheehan and C. M. Lieber, *Science*, 1997, **277**, 1971; H. Hoffmann, I. Utke, B. Moser, J. Michler, S. H. Christiansen, V. Schmidt, S. Senz, P. Werner, U. Gosele and C. Ballif, *Nano Lett.*, 2006, **6**, 622; H. Ni and X. D. Li, *Nanotechnology*, 2006, **17**, 3591; P. X. Gao, W. J. Mai and Z. L. Wang, *Nano Lett.*, 2006, **6**, 2536.

107 J. H. Song, X. D. Wang, J. Liu, H. B. Liu, Y. L. Li and Z. L. Wang, *Nano Lett.*, 2008, **8**, 203; X. D. Wang, J. Liu, J. H. Song and Z. L. Wang, *Nano Lett.*, 2007, **7**, 2475; Y. Gao and Z. L. Wang, *Nano Lett*, 2007, **7**, 2499; Z. L. Wang and J. H. Song, *Science*, 2006, **312**, 242.

108 C. F. Pan, H. Wu, C. Wang, B. Wang, L. Zhang, Z. D. Cheng, P. Hu, W. Pan, Z. Y. Zhou, X. Yang and J. Zhu, *Adv. Mater.*, 2008, **20**, 1644.

109 B. Z. Tian, X. L. Zheng, T. J. Kempa, Y. Fang, N. F. Yu, G. H. Yu, J. L. Huang and C. M. Lieber, *Nature*, 2007, **449**, 885; T. Stelzner, M. Pietsch, G. Andra, F. Falk, E. Ose and S. Christiansen, *Nanotechnology*, 2008, **19**, 295203; M. D. Kelzenberg, D. B. Turner-Evans, B. M. Kayes, M. A. Filler, M. C. Putnam, N. S. Lewis and H. A. Atwater, *Nano Lett.*, 2008, **8**, 710; E. C. Garnett and P. D. Yang, *J. Am. Ceram. Soc.*, 2008, **130**, 9224; L. Tsakalakos, J. Balch, J. Fronheiser, B. A. Korevaar, O. Sulima and J. Rand, *Appl. Phys. Lett.*, 2007, **91**, 233117.

110 K. Q. Peng, Y. Xu, Y. Wu, Y. J. Yan, S. T. Lee and J. Zhu, *Small*, 2005, **1**, 1062.

111 H. Fang, X. D. Li, S. Song, Y. Xu and J. Zhu, *Nanotechnology*, 2008, **19**, 255703; H. Fang, K. Q. Peng, Y. Wu, S. Song, Y. Xu and J. Zhu, *Acta Energiae Solaris Sinica (in Chinese edition)*, 2008, in press; H. Fang, Y. Wu and J. Zhu, *J. Mater. Res.*, 2008, in press.

